Scientific Research Publishing

International Journal of Organic Chemistry, 2018, 8, 54-83
http://www.scirp.org/journal/ijoc
ISSN Online: 2161-4695
ISSN Print: 2161-4687

The Application of New Chiral Ferrocene Ligands in Asymmetric Transfer Hydrogenation of Ketones

Yuan-Zhao Mo, Quan-Jun Wang, Hui-Fang Nie, Qiao-Feng Wang*

School of Pharmacy, the Fourth Military Medical University, Xi'an, China
Email: *zytwqf@fmmu.edu.cn

How to cite this paper: Mo, Y.-Z., Wang, Q.-J., Nie, H.-F. and Wang, Q.-F. (2018) The Application of New Chiral Ferrocene Ligands in Asymmetric Transfer Hydrogenation of Ketones. *International Journal of Organic Chemistry*, **8**, 54-83.
https://doi.org/10.4236/ijoc.2018.81004

Received: December 6, 2017
Accepted: February 20, 2018
Published: February 23, 2018

Copyright © 2018 by authors and Scientific Research Publishing Inc.
This work is licensed under the Creative Commons Attribution International License (CC BY 4.0).
http://creativecommons.org/licenses/by/4.0/

Open Access

Abstract

Four easily available ferrocenyl chiral ligands have been screened firstly for ruthenium (II)-catalyzed asymmetric transfer hydrogenation of acetophenone with HCOOH/Et_3N azeotrope as the hydrogen source. A moderate chemical yield of 1-phenylethanol with 83% ee was obtained when (R_C, S_{Fc})-1-(Diphenylphosphino)-2-[1-*N*-(3-methylpyridin-2-ylmethyl) ethyl] ferrocene (**L_1**) was used. Particularly, both ruthenium and iridium could coordinate with **L_1** to accomplish the asymmetric reduction of series of aromatic ketones separately. The desired products were achieved with up to 86% ee.

Keywords

Asymmetric Transfer Hydrogenation, Ferrocene, Ligand, Ketone

1. Introduction

Asymmetric transfer hydrogenation (ATH) often has been achieved by the help of the combination of transition metal and chiral ligands [1] [2] [3]. In the field, the exploration of new ligands or the new utilization of reported ones always attracted researcher's interest. Ferrocene-based chiral complexes generally played important roles in asymmetric reactions due to ferrocene's highly electron donating property as well as the unique structure [4] [5] [6] [7]. However, it should be noticed that most of the ATH catalyzed by chiral ferrocene derived catalysts used isopropanol as the hydrogen donor. Formic acid, as a more effective hydrogen donor for its irreversible kinetic enantioselectivity seldom collocated with ferrocenyl chiral ligands in ATH [8]-[13]. Furthermore, as far as transition metal in ATH was concerned, ruthenium and iridium could both be employed

in ATH [14] [15] [16] [17]. Commonly, different transition metals' coordination with the same chiral ligand provides more possibility for more stereoinduction [18] [19] [20] [21] [22]. Therefore, chiral ferrocenyl derivatives' ($\mathbf{L_1}$-$\mathbf{L_4}$, Figure 1) combination with the HCOOH hydrogen donor and its integration with two transition metals are both investigated. The results indicated that the ATH of aryl ketone could proceed smoothly at the presence of $\mathbf{L_1}$-$\mathbf{L_4}$ and formic acid. Among them, the reaction with $\mathbf{L_1}$-metal complex existed gave the best chemical yield and optical yield.

2. Experimental

2.1. General

All reactions involving air- or moisture-sensitive species were finished under N_2 atmosphere. Solvents were dried by standard methods and freshly distilled before use if needed. All other chemicals were used as purchased. $\mathbf{L_1}$-$\mathbf{L_4}$ were prepared from (*R*)-Ugi's amine according the published reports [23]. NMR spectra were recorded on a Bruker AV-400 spectrometer with TMS as an internal reference. Chiral High Performance Liquid Chromatography (HPLC) analyses were completed with an Agilent 1200 series apparatus and Chiralpak OD-H and OJ-H columns. The configuration of the products was determined by comparison to the literature data.

2.2. The General Procedure for ATH in HCOOH/Et_3N (5:2)

A Schlenk flask was charged with substrate (1 mmol), [Ru (*p*-cymene) $Cl_2]_2$ (0.0025 mmol) or [{IrCl (COD)}$_2$] (0.0025 mmol), chiral ligand (0.005 mmol) in 1 mL solvent and stirred at r.t. for 4 hours under N_2 atmosphere. After that, 4 mL HCOOH/Et_3N azeotrope was injected by syringe. The mixture went on stirring at −20˚C for 48 h under N_2. Subsequently, saturated $NaHCO_3$ (5 mL) and H_2O (5 mL) were added and the mixture was then extracted with EtOAc (10 mL) for three times and dried over by Na_2SO_4. Then after column chromatography, the pure product was got and identified by ^{1}H NMR. The analytical data

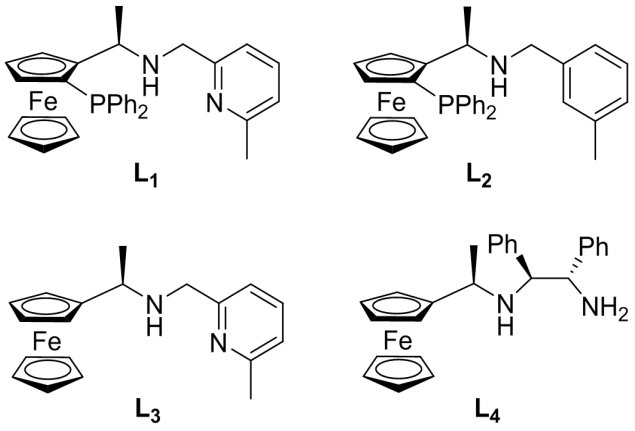

Figure 1. Ferrocene-based chiral ligands $\mathbf{L_1}$-$\mathbf{L_4}$.

were given in supporting information.

3. Results and Discussion

L_1-**L_4**'s synthesis could be accomplished according to our published report [23]. Once these ligands in hands, a preliminary study should be carrying out. Firstly, we have used **L_1** with $RuCl_2$ (*p*-cymene) as catalyst while acetophenone (**1a**) was substrate to optimize the reaction efficiency. Various solvents, different temperatures and the ratios of catalyst/substrate (C/S) were tested. The results were listed in Table 1.

The data in Table 1 showed that the solvent had influence on the experiment. For example, only trace conversion happened in MeOH, CH_2Cl_2 and THF (Table 1, entry 1-3). Another three solvents (EtOAc, *t*-BuOMe, DMF) gave better chemical yields and better enantioselectivities. Among them, DMF provided the highest ee and chemical yield (Table 1, entry 1-6). So DMF was chosen as the optimized solvent for further experiments.

In DMF, ATH of **1a** were conducted at different temperatures that ranged from r.t. to −40˚C. Compared with r.t., −20˚C was proved to be a suitable reaction temperature with the improved ee value (Table 1, entry 6 vs. 7). However, when the temperature decreased to −40˚C, only trace products could be observed (Table 1, entry 8). So the rest of experiments were completed at −20˚C.

Table 1. The ATH reactions catalyzed by **L_1** with [$RuCl_2$ (*p*-cymene)]$_2$.

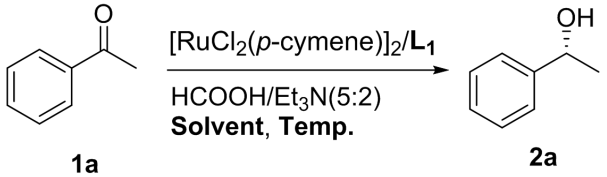

Entry	Solvent	C/S	Temp.	Yield (%)[d]	Ee (%)[e]
1[a]	MeOH	0.5%	r.t.	Trace	ND
2[a]	CH_2Cl_2	0.5%	r.t.	Trace	ND
3[a]	THF	0.5%	r.t.	Trace	ND
4[a]	EtOAc	0.5%	r.t.	27	45
5[a]	*t*-BuOMe	0.5%	r.t.	42	60
6[a]	DMF	0.5%	r.t.	74	79
7	DMF	0.5%	-20˚C	66	84
8	DMF	0.5%	-40˚C	Trace	ND
9[b]	DMF	0.25%	-20˚C	38	75
10[c]	DMF	1%	-20˚C	72	83

[a]The mixture of 1 mmol of **1a**, 0.0025 mmol of [$RuCl_2$(*p*-cymene)]$_2$ and 0.005 mmol of **L_1** in 4 mL HCOOH/Et_3N (5:2) azeotrope and 1 mL solvent at r.t. was stirred for 48 h; [b]Cat. (0.25 mol %); [c]Cat. (1 mol %); [d]Isolated yields after column chromatography; [e]The ee values was determined by chiral HPLC with Chiralpak OD-H column and the configuration was assigned by comparing the optical rotation with reported values [24] [25] [26] [27].

Additionally, the change of C/S from 0.5% to 0.25% caused a lower chemical yield and lessened ee (Table 1, entry 9). But the bigger ratio did not mean the improved results. When the ratio was 1%, the yield was raised slightly and the ee value was almost the same as that of 0.5% C/S (Table 1, entry 7 vs. entry 10). Therefore, the 0.5% of C/S was reasonable for next work.

Under the optimized conditions, the ligands structure effect on the ATH was also screened. The corresponding results were shown in Table 2. $\mathbf{L_1}$ with P, N, N elements and planar chirality gave the best optical selectivity (84% ee) (Table 2, entry 1). $\mathbf{L_2}$'s result (81% ee) was a little worse than $\mathbf{L_1}$'s (Table 2, entry 2). It implied that N atom on pyridine unit of $\mathbf{L_1}$ had positive effect on the stereoinduction and the yield. The behaviors of $\mathbf{L_3}$, $\mathbf{L_4}$ were both worse. $\mathbf{L_3}$'s racemic result was not surprising for the reason that there was only one stereogenic center in $\mathbf{L_3}$ (Table 2, entry 3). $\mathbf{L_4}$ gave (*S*)-products with 37% ee (Table 2, entry 4). The configuration of moiety in $\mathbf{L_4}$ is also (*S*, *S*). This indicated that the configuration of the product was controlled by the chiral diamine moiety in ligand structure. The chirality of Uig's amine had not apparent contribution to the stereocontrol. Altogether, the planer chiral elements and the P unit on the ferrocene ring were essential for a higher enantioselectivities. As far as the chemical yields were concerned, the four ligands' performance was almost similar. Lastly, $\mathbf{L_1}$ was choosed to be examined for various ketones' ATH.

As Table 3 summarized, for $\mathbf{L_1}$-Ru or $\mathbf{L_1}$-Ir catalyst, the reactions of acetophenone derivatives proceed smoothly. The ee values ranged from 66% to 86%. First, the position of the ring substituents had influence on the enantioselectivity. Then it seems that electronic properties of the ring substituents had no effect on the results because 3-methoxyacetophenone or 3'-(trifluoromethyl) acetophenone almost obtained the paralleled stereoselectivity (Table 3, entry 4, 5). Furthermore, for halogen substituted substrates, with the increase of atomic number of halogen, the ees of the reaction had a little increase (Table 3, entry

Table 2. The screen of $\mathbf{L_1}$-$\mathbf{L_4}$ with [$RuCl_2$ (*p*-cymene)]$_2$ in the ATH.

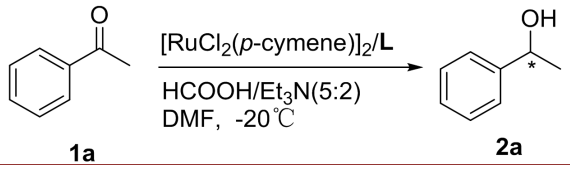

1a **2a**

Entry[a]	Ligand	Yield (%)[b]	Ee (%)(Conf.)[c]
1	$\mathbf{L_1}$	66	84(*R*)
2	$\mathbf{L_2}$	55	81(*R*)
3	$\mathbf{L_3}$	65	*Rac*
4	$\mathbf{L_4}$	50	37(*S*)

[a]1 mmol of **1a** with 0.0025 mmol of [$RuCl_2$(*p*-cymene)]$_2$, 0.005 mmol of ligand, 4 mL HCOOH/Et_3N (5:2) and 1 mL DMF was stirred for 48 h at −20˚C; [b]Isolated yields after column chromatography; [c]The ee and configuration of product were determined by chiral HPLC and according to literature [24] [25] [26] [27].

Table 3. The ATH of aromatic ketones catalyzed by $\mathbf{L_1}$-Ru or $\mathbf{L_1}$-Ir catalyst.

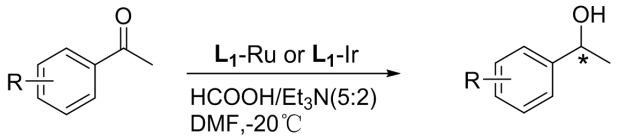

1a-1h 2a-2h

Entry	R	Product	Yield/ee (%)[a]	Yield/ee (%)[b]
1[c]	H	**2a**	66/84(*R*)	60/83(*R*)
2[c]	2-Br	**2b**	60/66(*R*)	65/77(*R*)
3[c]	3-Br	**2c**	63/76(*R*)	65/82(*R*)
4[c]	3-CF_3	**2d**	57/79(*R*)	62/85(*R*)
5[c]	3-OMe	**2e**	60/80(*R*)	68/81(*R*)
6[c]	4-F	**2f**	55/67(*R*)	60/70(*R*)
7[c]	4-Cl	**2g**	65/84(*R*)	60/72(*R*)
8[c]	4-Br	**2h**	66/86(*R*)	55/76(*R*)

[a]1 mmol of **1** with 0.0025 mmol of $[RuCl_2(p\text{-cymene})]_2$, 0.005 mmol of $\mathbf{L_1}$, 4 mL HCOOH/Et_3N (5:2) and 1 mL DMF was stirred for 48 h at −20˚C; [b]1 mmol of **1** with 0.0025 mmol of $[IrCl_2(COD)_2]$, 0.005 mmol of $\mathbf{L_1}$, 4 mL HCOOH/Et_3N (5:2) and 1 mL DMF was stirred for 48 h at −20˚C; [c]The yield was isolated yields after column chromatography. The ee and configuration of product were determined by chiral HPLC with Chiralpak OD-H or OJ-H. The absolute configuration was determined by comparison of the sign of optical rotation or retention time with 1iterature data [24] [25] [26] [27].

6-8). All the chemical yields reached moderate (55% - 68%). In addition, almost no difference existed between the performance of Ru and Ir catalyst in the ATH of various substrates.

4. Conclusion

In conclusion, we have demonstrated four chiral ferrocene-based ligands' utilization in ATH of aromatic ketones. Herein, HCOOH/Et_3N (5:2) system was firstly applied in this kind of reduction with chiral ferrocenyl ligands complexes existed. Both ruthenium and iridium could coordinate with $\mathbf{L_1}$ and could realize the reduction of acetophenone derivatives. Moderate to good enantiomeric excesses and medium isolated yields were achieved. Further studies of these ligands in other catalytic reactions are currently underway.

Acknowledgments

Financial support from the National Natural Science Foundation of China (NSFC, Nos. 21102175) and the Natural Science Foundation of Shaanxi Province, China (No.2016JM8070) are gratefully acknowledged.

References

[1] Wu, M., Cheng, T.Y., Ji, M., and Liu, G.H. (2015) Ru-Catalyzed Asymmetric Transfer Hydrogenation of *α*-Trifluoromethylimines. The *Journal of Organic Chemistry,* **80**, 3708-3713. http://doi.org/10.1021/acs.joc.5b00177

[2] Seo, Y.J., Kim, J.A. and Lee, H.K. (2015) Stereoselective Synthesis of 4-Substituted Cyclic Sulfamidate-5-Phosphonates by Using Rh-Catalyzed, Asymmetric Transfer Hydrogenation with Accompanying Dynamic Kinetic Resolution. The *Journal of Organic Chemistry,* **80**, 8887-8902. http://doi.org/10.1021/acs.joc.5b01434

[3] Lee, D.M., Kwak, S.H. and Lee, K.I. (2009) Highly Enantioselective Rh-Catalyzed Transfer Hydrogenation of α-Functionalized Arylketones. *Bulletin of the Korean Chemical Society*, **30**, 1317-1324. http://doi.org/10.5012/bkcs.2009.30.6.1317

[4] Dai, L.X., Tu, T., You, S.L., Deng, W.P. and Hou, X.L. (2003) Asymmetric Catalysis with Chiral Ferrocene Ligands. *Accounts of Chemical Research*, **36**, 659-667. http://doi.org/10.1021/ar020153m

[5] Hellmuth, T., Rieckhoff, S., Weiss, M., Dorst, K., Frey, W. and Peters, R. (2014) Cooperative Bimetallic Asymmetric Catalysis: Comparison of a Planar Chiral Ruthenocene Bis-Palladacycle to the Corresponding Ferrocene. *ACS Catalysis*, **4**, 1850-1858. http://doi.org/10.1021/cs500393x

[6] Zhou, Y., Zhu, F.L., Liu, Z.T., Zhou, X.M. and Hu, X.P. (2016) Chiral Ferrocenyl P,N-Ligands for Palladium-Catalyzed Asymmetric Formal [3 + 2] Cycloaddition of Propargylic Esters with β-Ketoesters: Access to Functionalized Chiral 2,3-Dihydrofurans. *Organic Letters,* **18**, 2734-2737. http://doi.org/10.1021/acs.orglett.6b01192

[7] Gao, D.W., Shi, Y.C., Gu, Q., Zhao, Z.L. and You, S.L. (2013) Enantioselective Synthesis of Planar Chiral Ferrocenes via Palladium-Catalyzed Direct Coupling with Arylboronic Acids. *Journal of the American Chemical Society,* **135**, 86-89. http://doi.org/10.1021/ja311082u

[8] Isik, U., Aydemir, M., Meric, N., Durap, F., Kayan, C., Temel, H. and Baysal, A. (2013) Tunable Ferrocenyl-Phosphinite Ligands for the Ruthenium(II)-Catalyzed Asymmetric Transfer Hydrogenation of Ketones. *Journal of Molecular Catalysis A*: *Chemical,* **379**, 225-233. https://doi.org/10.1016/j.molcata.2013.08.005

[9] Mejía, E., Aardoom, R. and Togni, A. (2012) Asymmetric Transfer Hydrogenation of Ketones Catalyzed by Rhenium Complexes with Chiral Ferrocenylphosphane Ligands. *European Journal of Inorganic Chemistry,* **2012**, 5021-5032. https://doi.org/10.1002/ejic.201200693

[10] Baratta, W., Chelucci, G., Herdtweck, E., Magnolia, S., Siega, K. and Rigo, P. (2007) Highly Diastereoselective Formation of Ruthenium Complexes for Efficient Catalytic Asymmetric Transfer Hydrogenation. *Angewandte Chemie International Edition*, **46**, 7651-7654. https://doi.org/10.1002/anie.200702278

[11] Bünyamin, A.K., Aydemir, M., Durap, F., Meriç, N., Elma, D. and Baysal, A. (2015) Highly Efficient Iridium Catalysts Based on C_2-Symmetric Ferrocenyl Phosphinite Ligands for Asymmetric Transfer Hydrogenations of Aromatic Ketones. *Tetrahedron*: *Asymmetry,* **26**, 1307-1313. https://doi.org/10.1016/j.tetasy.2015.10.002

[12] Bünyamin, A.K., Aydemir, M., Durap, F., Meriç, N., Elma, D. and Baysal, A. (2015) The First Application of C_2-Symmetric Ferrocenyl Phosphinite Ligands for Rhodium-Catalyzed Asymmetric Transfer Hydrogenation of Various Ketones. *Inorganica Chimica Acta*, **438**, 42-51. https://doi.org/10.1016/j.ica.2015.09.003

[13] Ikariya, T. and Blacker, A.J. (2007) Asymmetric Transfer Hydrogenation of Ketones with Bifunctional Transition Metal-Based Molecular Catalysts. *Account. Chemical. Research,* **40**, 1300-1308. http://doi.org/10.1021/ar700134q

[14] Morris, D.M., McGeagh, M., De Peña, D. and Merola, J.S. (2014) Extending the Range of Pentasubstituted Cyclopentadienyl Compounds: The Synthesis of a Series

of Tetramethyl(Alkyl or Aryl)Cyclopentadienes (Cp^{*R}), Their Iridium Complexes and Their Catalytic Activity for Asymmetric Transfer Hydrogenation. *Polyhedron*, **84**, 120-135. https://doi.org/10.1016/j.poly.2014.06.053

[15] Malacea, R., Poli, R. and Manoury, E. (2010) Asymmetric Hydrosilylation, Transfer Hydrogenation and Hydrogenation of Ketones Catalyzed by Iridium Complexes. *Coordination Chemistry Reviews*, **254**, 729-752. https://doi.org/10.1016/j.ccr.2009.09.033

[16] Zerla, D., Facchett, G., Fusè, M., Pellizzoni, M., Castellano, C., Cesarotti, E., Gandolfi, R. and Rimoldi, I. (2014) 8-Amino-5,6,7,8-Tetrahydroquinolines as Ligands in Iridium(III) Catalysts for the Reduction of Aryl Ketones by Asymmetric Transfer Hydrogenation (ATH). *Tetrahedron*: *Asymmetry*, **25**, 1031-1037. https://doi.org/10.1016/j.tetasy.2014.06.003

[17] Popoola, S.A., Jaseer, E.A., Al-Saadi, A.A., Polo, V., Casado, M.A. and Oro, L.A. (2015) Iridium Complexes as Catalysts in the Hydrogen Transfer of Isopropanol to Acetophenone: Ligand Effects and DFT Studies. *Inorganica Chimica Acta*, **436**, 146-151. https://doi.org/10.1016/j.ica.2015.07.031

[18] Kenichi, K., Kota, T., Hidehiro, U., Shibata, Y. and Tanaka, K. (2016) Rhodium-Catalyzed Atroposelective [2 + 2 + 2] Cycloaddition of *Ortho*-Substituted Phenyl Diynes with Nitriles: Effect of *Ortho* Substituents on Regio- and Enantioselectivity. *Organic Letters,* **18**, 2170-2173. http://doi.org/10.1021/acs.orglett.6b0079

[19] Liang, T., Zhang, W.D. and Michael, J.K. (2015) Iridium-Catalyzed C–C Coupling of a Simple Propargyl Ether with Primary Alcohols: Enantioselective Homoaldol Addition via Redox-Triggered (*Z*)-Siloxyallylation. *Journal of the American Chemical Society,* **137**, 16024-16027. http://doi.org/10.1021/jacs.5b12131

[20] Meng, J.J., Lv, M.G. and Zhang, X.M. (2015) Highly Enantioselective Hydrogenation of o-Alkoxy Tetrasubstituted Enamides Catalyzed by a Rh/(*R*,*S*)-JosiPhos Catalyst. *Organic Letters*, **17**, 1842-1845. http://doi.org/10.1021/acs.orglett.5b00401

[21] Kobayashi, K., Yamamoto, Y. and Miyaura, N. (2011) Pd/Josiphos-Catalyzed Enantioselective *α*-Arylation of Silyl Ketene Acetals and Mechanistic Studies on Transmetalation and Enantioselection. *Organometallics*, **30**, 6323-6327. http://doi.org/10.1021/om200945q

[22] Kevin, G.M.K., Diane, N.L. and Dong, V.M. (2014) Rh(I)-Catalyzed Intermolecular Hydroacylation: Enantioselective Cross-Coupling of Aldehydes and Ketoamides. *Journal of the American Chemical Society*, **136**, 9471-9476. http://doi.org/10.1021/ja504296x

[23] Mo, Y.Z., Nie, H.F., Lei, Y., Zhang, D.X., Li, X.Y., Zhang, S.Y. and Wang Q.F. (2016) Asymmetric Transfer Hydrogenation of γ-Aryl α,γ-Dioxo-Butyric Acid Esters. *RSC Advances*, **6**, 33126-33131. http://doi.org/10.1039/C6RA02500E

[24] Zoabi, A., Omar, S. and Abu-Reziq, R. (2015) Chiral Ruthenium Catalyst Immobilized within Magnetically Retrievable Mesoporous Silica Microcapsules for Aqueous Asymmetric Transfer Hydrogenations. *European Journal of Inorganic Chemistry*, **12**, 2101-2109. http://doi.org/10.1002/ejic.201403212

[25] Han, M.L., Hub, X.P., Huang, J.D., Chen, L.G. and Zheng, Z. (2011) New Chiral Amino Alcohol Ligands Derived from 1-Phenylethylamine for Efficient Ru-Catalyzed Asymmetric Transfer Hydrogenation. *Tetrahedron*: *Asymmetry*, **22**, 222-225. https://doi.org/10.1016/j.tetasy.2011.01.017

[26] Xie, J.H., Liu, X.Y., Xie, J.B., Wang, L.X. and Zhou, Q.L. (2011) An Additional Coordination Group Leads to Extremely Efficient Chiral Iridium Catalysts for

Asymmetric Hydrogenation of Ketones. *Angewandte Chemie International Edition*, **50**, 7329-7332. https://doi.org/10.1002/anie.201102710

[27] Chen, Y.C., Wu, T.F., Deng, J.G., Liu, H., Cui, X., Zhu, J., Jiang, Y.Z., Michael, C.K.C. and Albert, S.C.C. (2002) Multiple Dendritic Catalysts for Asymmetric Transfer Hydrogenation. *The Journal of Organic Chemistry*, **67**, 5301-5306. http://doi.org/10.1021/jo0257795

Supplementary Materials

1. Copies of the HPLC spectra of the catalysis products 2 [catalysts were ferrocene-based chiral ligands with Ru-complex]

1) Table 1

1-Phenylethanol (2a)

27% yield, 45% ee in EtOAc. 42% yield, 60% ee in *t*-BuOMe.74% yield, 79% ee in DMF at r.t. 66% yield, 84% ee in DMF at −20˚C. 38% yield, 75% ee in DMF at −20˚C with C/S = 0.25%, 72% yield, 84% ee in DMF at −20˚C with C/S = 1% for 48 h (ligand is $\mathbf{L_1}$), determined by HPLC analysis (Chiralcel OD-H column, Hexane/i-PrOH = 95/5, Flow rate: 1 mL/min, UV detection at 215 nm).

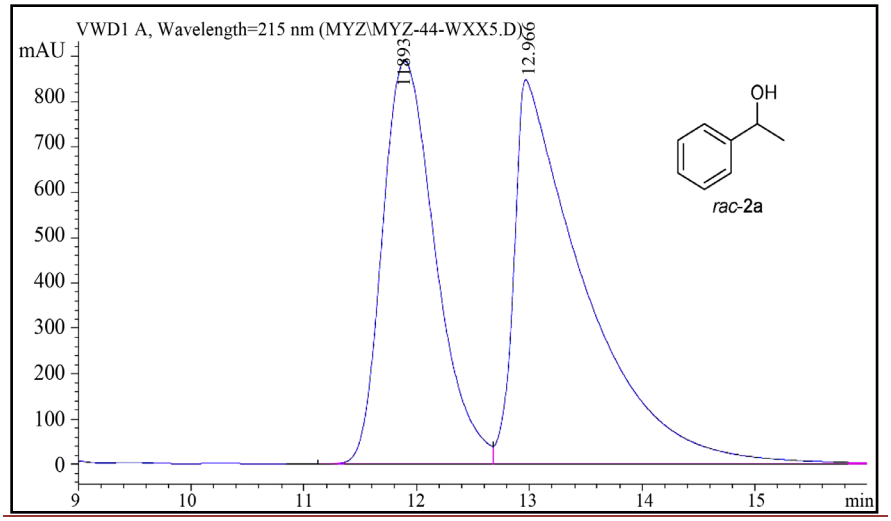

#	Time	Peak area	Peak height	Peak width	Symmetry factor	Peak area%
1	11.893	29038.4	888.2	0.5074	0.686	43.997
2	12.966	36961.5	847.8	0.5816	0.206	56.002

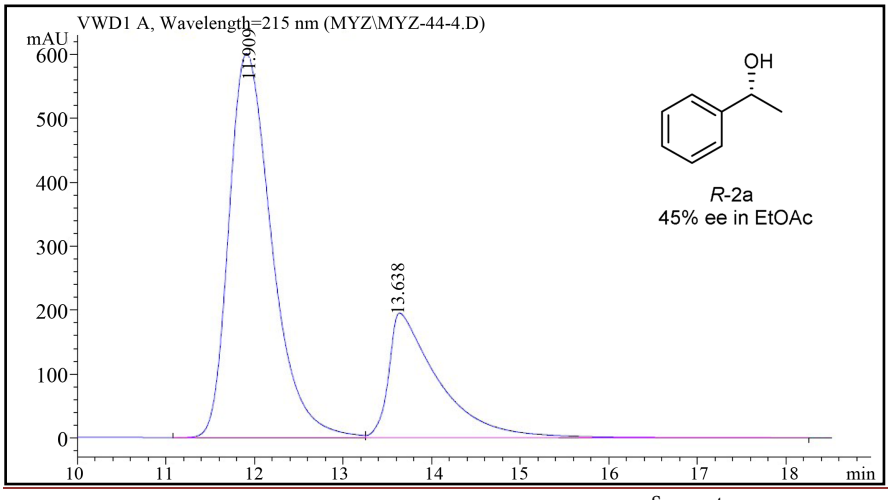

#	Time	Peak area	Peak height	Peak width	Symmetry factor	Peak area%
1	11.986	18454.8	546.6	0.5207	0.687	80.112
2	13.768	4581.6	131.6	0.5802	0.313	19.888

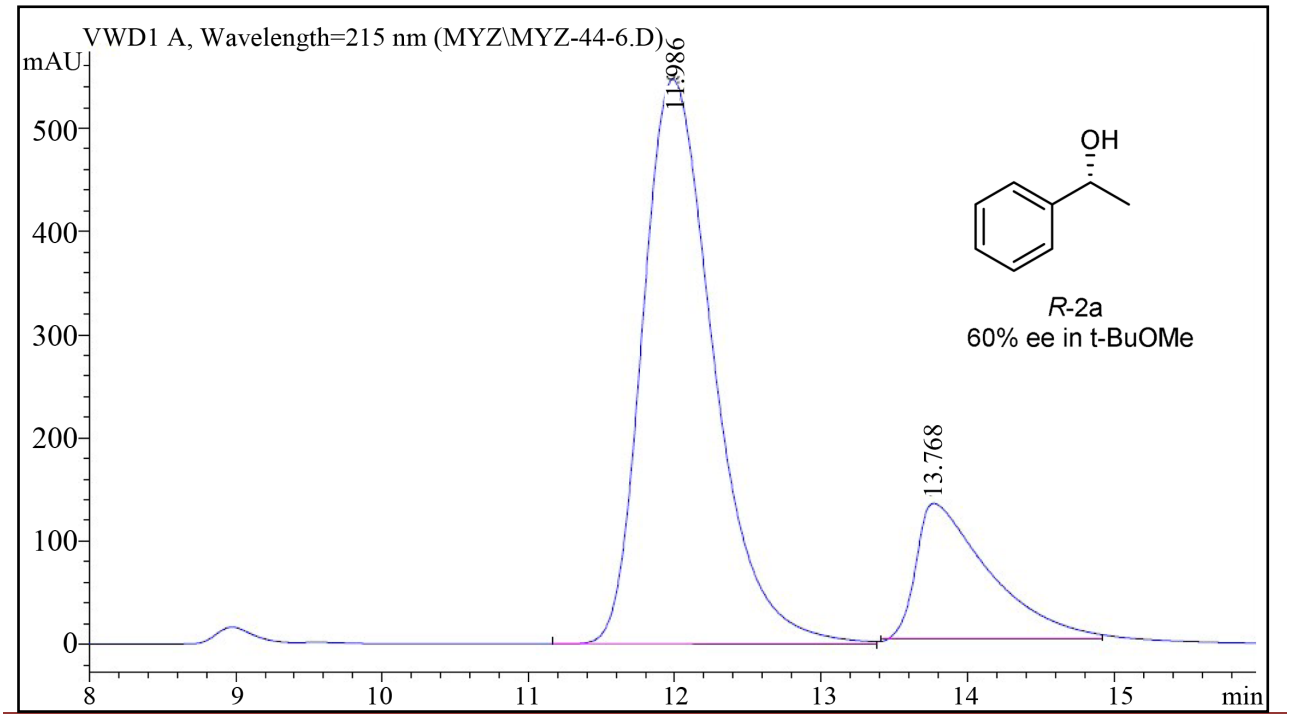

#	Time	Peak area	Peak height	Peak width	Symmetry factor	Peak area%
1	11.986	18454.8	546.6	0.5207	0.687	80.112
2	13.768	4581.6	131.6	0.5802	0.313	19.888

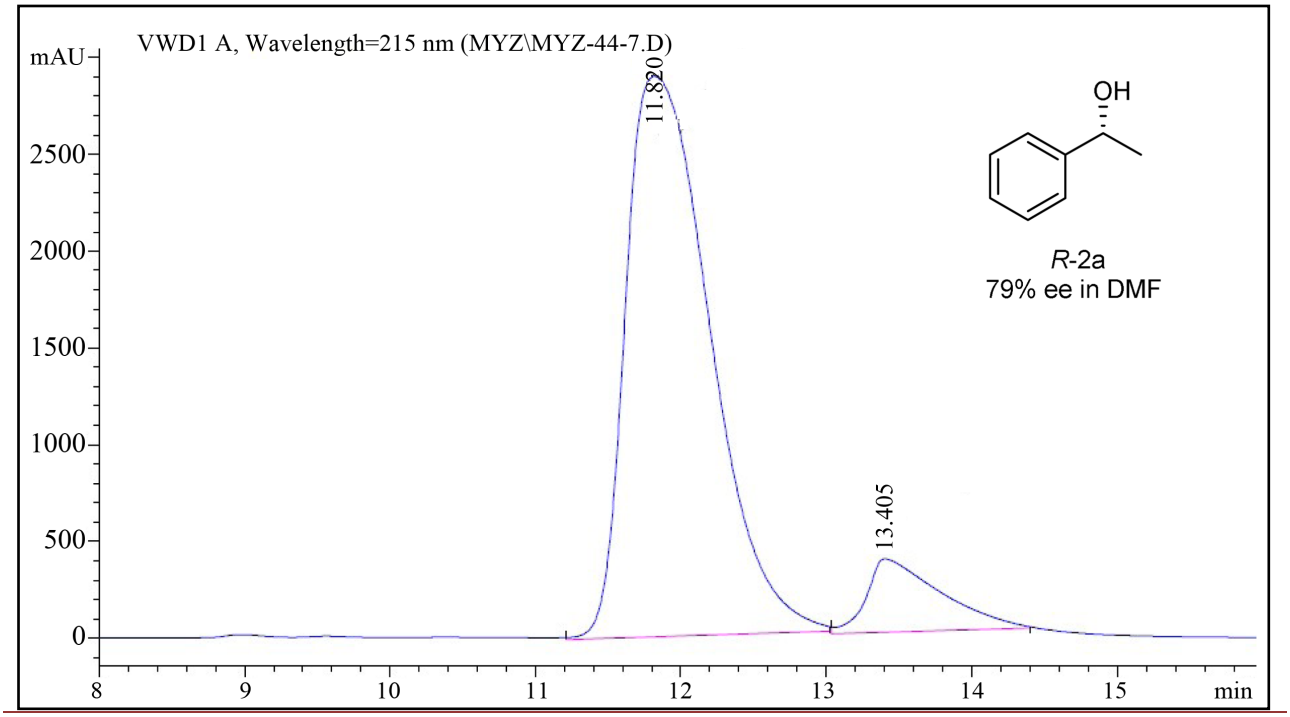

#	Time	Peak area	Peak height	Peak width	Symmetry factor	Peak area%
1	11.820	114774.7	2883.4	0.6708	0.515	89.6815
2	13.405	13416.2	379.8	0.5887	0.306	10.3185

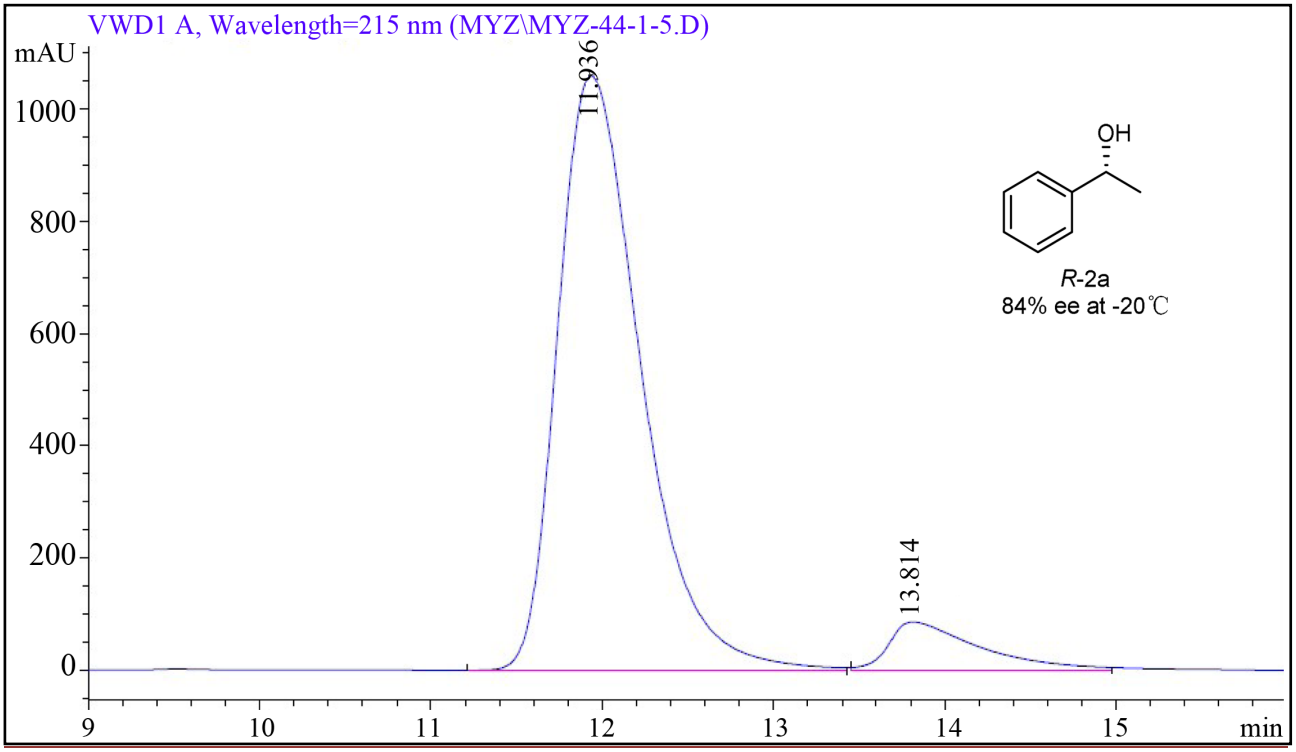

#	Time	Peak area	Peak height	Peak width	Symmetry factor	Peak area%
1	11.936	35732.5	1058.3	0.5222	0.627	92.037
2	13.814	3091.3	85.2	0.6048	0.365	7.9625

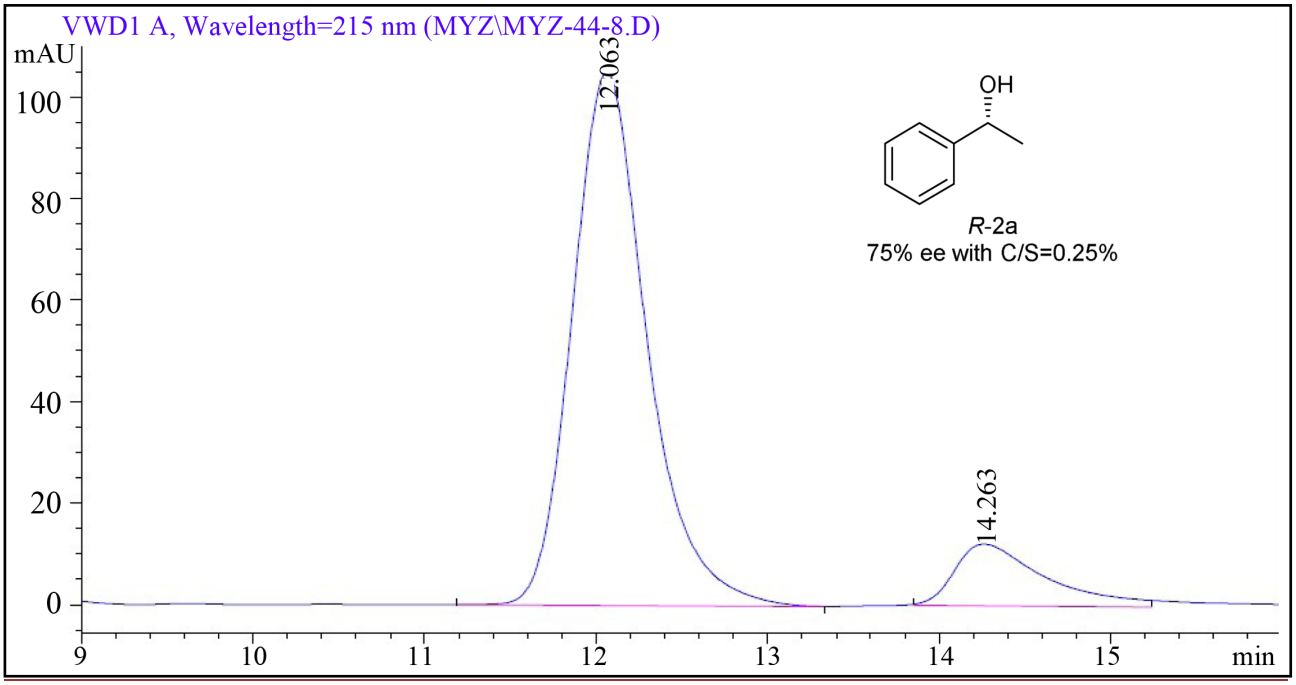

#	Time	Peak area	Peak height	Peak width	Symmetry factor	Peak area%
1	12.063	3184.1	104.9	0.463	0.799	87.759
2	14.263	444.1	12.1	0.6098	0.46	12.241

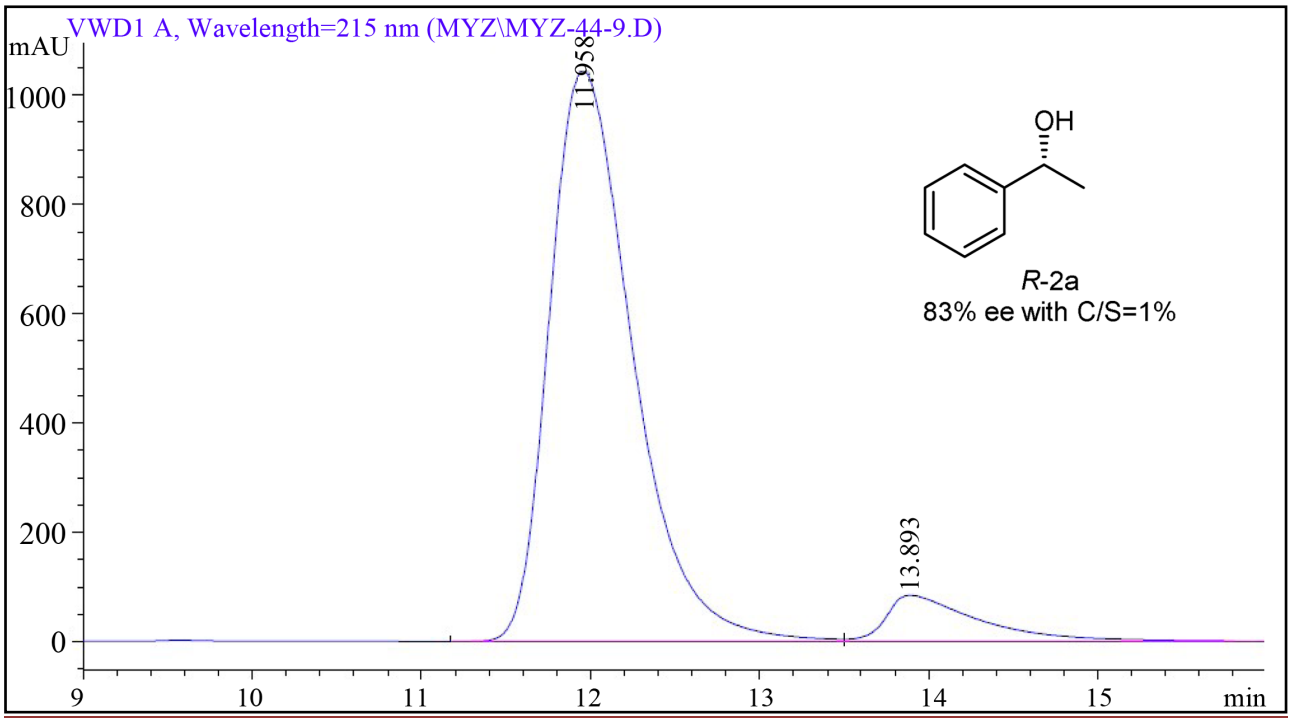

#	Time	Peak area	Peak height	Peak width	Symmetry factor	Peak area%
1	11.958	35762.6	1043.1	0.5299	0.628	91.557
2	13.893	3297.7	84.5	0.5524	0.327	8.442

2) Table 2

55% yield, 81% ee by L2 determined by HPLC analysis (Chiralcel OJ-H column, Hexane/i-PrOH = 90/10, Flow rate: 1 mL/min, UV detection at 215 nm). 65% yield, racemic by L3. 50% yield, 37% ee by L4 determined by HPLC analysis (Chiralcel OD-H column, Hexane/i-PrOH = 95/5, Flow rate: 1 mL/min, UV detection at 215 nm).

3) Table 3

a) 1-(2-bromophenyl)ethanol (2b)

60% yield, 66% ee determined by HPLC analysis (Chiralcel OJ-H column, Hexane/i-PrOH = 95/5, Flow rate: 1 mL/min, UV detection at 215 nm).

b) 1-(3-bromophenyl)ethanol (2c)

63% yield, 76% ee determined by HPLC analysis (Chiralcel OD-H column, Hexane/i-PrOH=98/2, Flow rate: 1 mL/min, UV detection at 215 nm).

c) 1-(3-(trifluoromethyl)phenyl)ethanol (2d)

57% yield, 79% ee determined by HPLC analysis (Chiralcel OD-H column, Hexane/i-PrOH = 98/2, Flow rate: 1 mL/min, UV detection at 215 nm).

d) 1-(3-methoxyphenyl)ethanol (2e)

60% yield, 80% ee determined by HPLC analysis (Chiralcel OD-H column, Hexane/i-PrOH = 95/5, Flow rate: 1 mL/min, UV detection at 215 nm).

e) 1-(4-fluorophenyl)ethanol (2f)

55% yield, 67% ee determined by HPLC analysis (Chiralcel OJ-H column, Hexane/i-PrOH = 95/5, Flow rate: 1 mL/min, UV detection at 215 nm).

f) 1-(4-chlorophenyl)ethanol (2g)

65% yield, 84% ee determined by HPLC analysis (Chiralcel OJ-H column, Hexane/i-PrOH = 95/5, Flow rate: 1 mL/min, UV detection at 215 nm).

g) 1-(4-bromophenyl)ethanol (2h)

66% yield, 86% ee determined by HPLC analysis (Chiralcel OJ-H column, Hexane/i-PrOH = 95/5, Flow rate: 1 mL/min, UV detection at 215 nm).

2. Copies of the HPLC spectra of the catalysis products 2 [catalysts were ferrocene-based chiral ligands with Ir-complex]

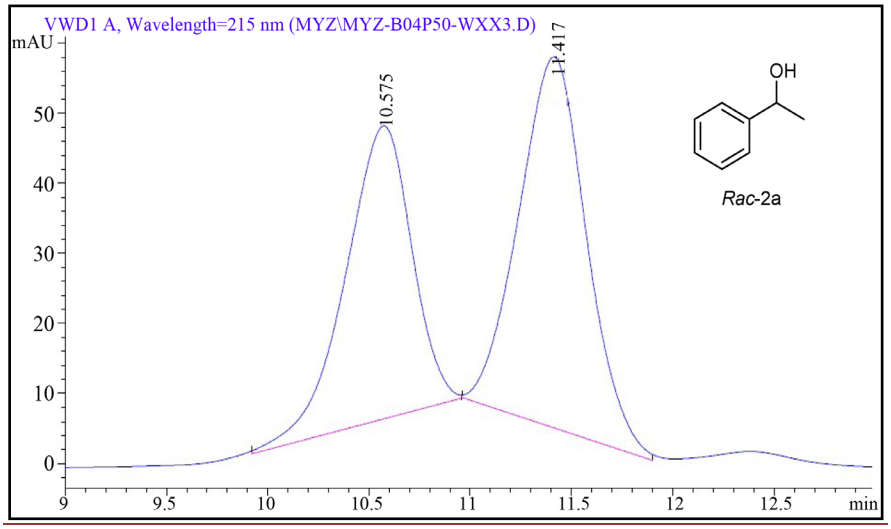

#	Time	Peak area	Peak height	Peak width	Symmetry factor	Peak area%
1	10.575	955.4	41.9	0.3803	1.352	43.628
2	11.417	1234.5	53	0.3882	1.022	56.372

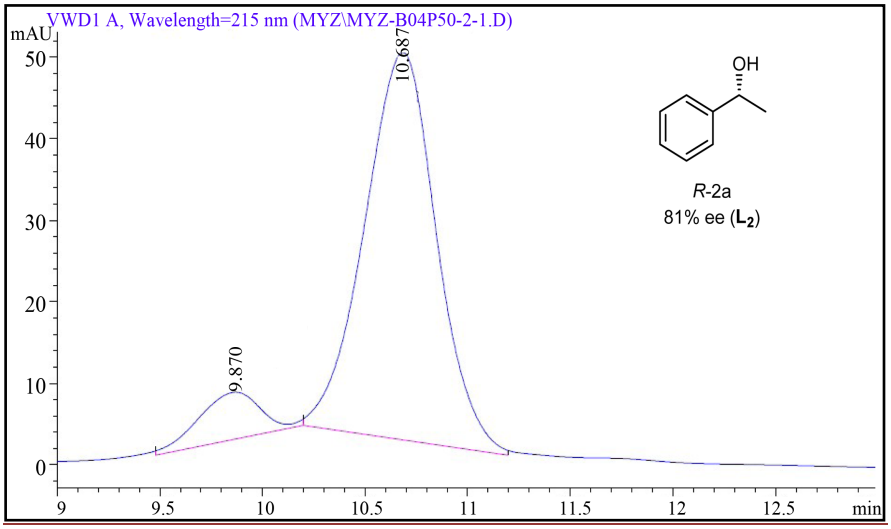

#	Time	Peak area	Peak height	Peak width	Symmetry factor	Peak area%
1	9.87	122.6	5.8	0.3552	1.523	9.581
2	10.687	1157.5	47.5	0.4058	1.093	90.419

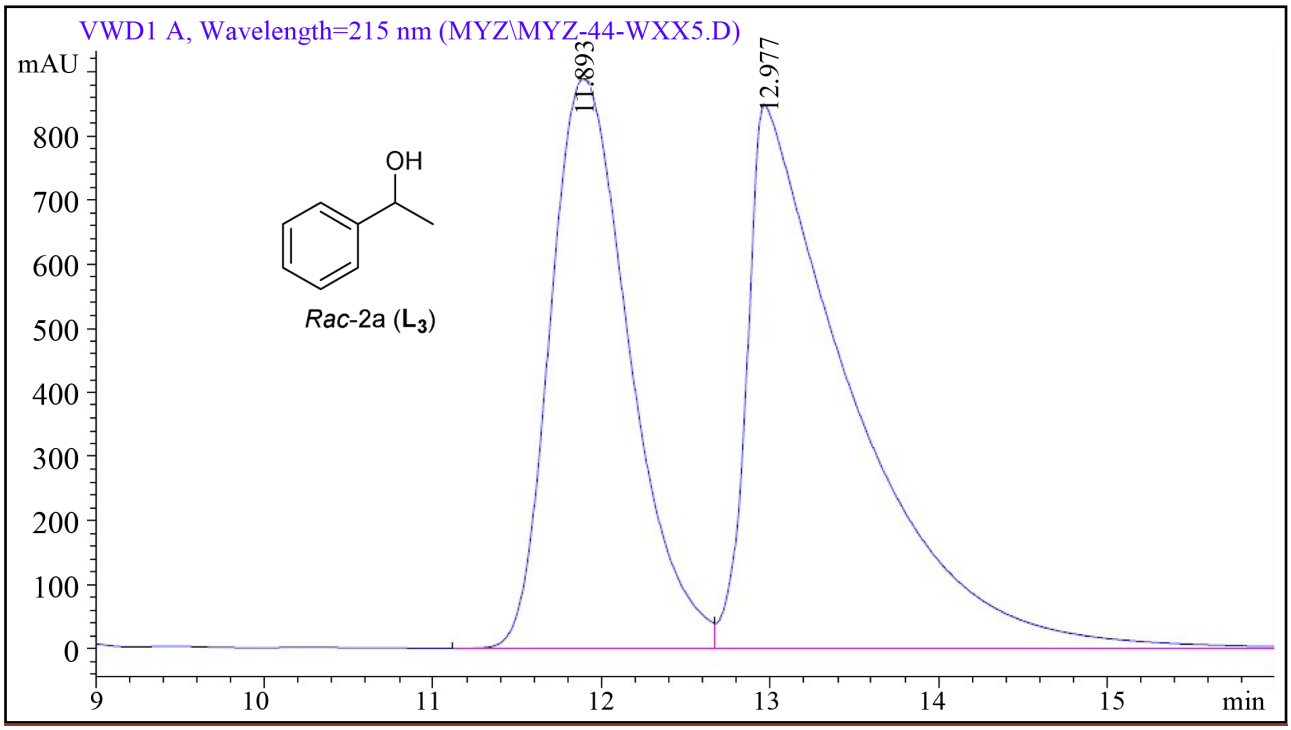

#	Time	Peak area	Peak height	Peak width	Symmetry factor	Peak area%
1	11.893	29031.1	888.15	0.5054	0.686	43.98
2	12.977	36978.3	844.21	0.5870	0.206	56.01

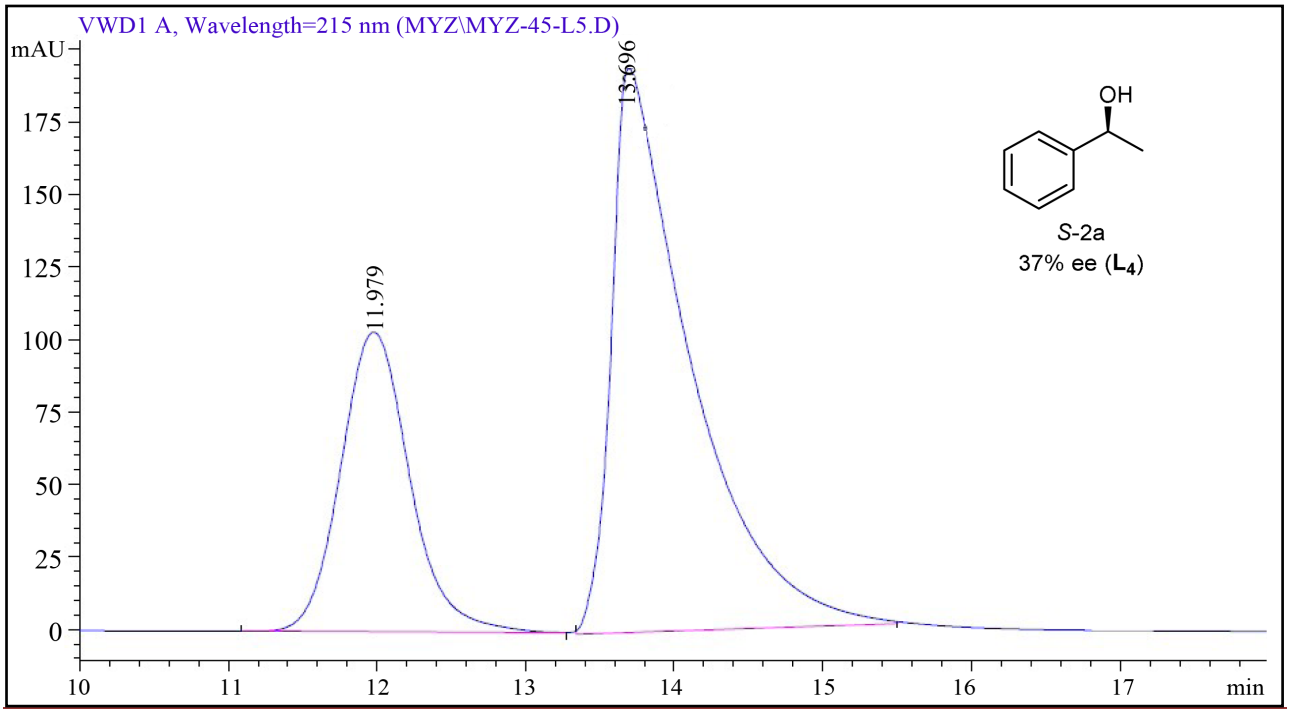

#	Time	Peak area	Peak height	Peak width	Symmetry factor	Peak area%
1	11.979	3335.1	103.3	0.5006	0.866	31.534
2	13.696	7241.1	194.7	0.6198	0.268	68.466

Table 3

1) 1-Phenylethanol (2a)

60% yield, 83% ee determined by HPLC analysis (Chiralcel OJ-H column, Hexane/i-PrOH = 90/10, Flow rate: 1 mL/min, UV detection at 215 nm)

2) 1-(2-bromophenyl)ethanol (2b)

65% yield, 77% ee determined by HPLC analysis (Chiralcel OJ-H column, Hexane/i-PrOH = 95/5, Flow rate: 1 mL/min, UV detection at 215 nm).

3) 1-(3-bromophenyl)ethanol 2c)

65% yield, 82% ee determined by HPLC analysis (Chiralcel OJ-H column, Hexane/i-PrOH = 99/1, Flow rate: 1 mL/min, UV detection at 215 nm).

4) 1-(3-(trifluoromethyl)phenyl)ethanol (2d)

62% yield, 85% ee determined by HPLC analysis (Chiralcel OJ-H column, Hexane/i-PrOH = 99/1, Flow rate: 1 mL/min, UV detection at 215 nm).

5) 1-(3-methoxyphenyl)ethanol (2e)

68% yield, 81% ee determined by HPLC analysis (Chiralcel OJ-H column, Hexane/i-PrOH = 98/2, Flow rate: 1 mL/min, UV detection at 215 nm).

6) 1-(4-fluorophenyl)ethanol (2f)

60% yield, 70% ee determined by HPLC analysis (Chiralcel OJ-H column, Hexane/i-PrOH = 99/1, Flow rate: 1 mL/min, UV detection at 215 nm).

7) 1-(4-chlorophenyl)ethanol (2g)

60% yield, 72% ee determined by HPLC analysis (Chiralcel OJ-H column, Hexane/i-PrOH = 99/1, Flow rate: 1 mL/min, UV detection at 215 nm).

8) 1-(4-bromophenyl)ethanol (2h)

55% yield, 76% ee determined by HPLC analysis (Chiralcel OJ-H column, Hexane/i-PrOH=98/2, Flow rate: 1 mL/min, UV detection at 215 nm).

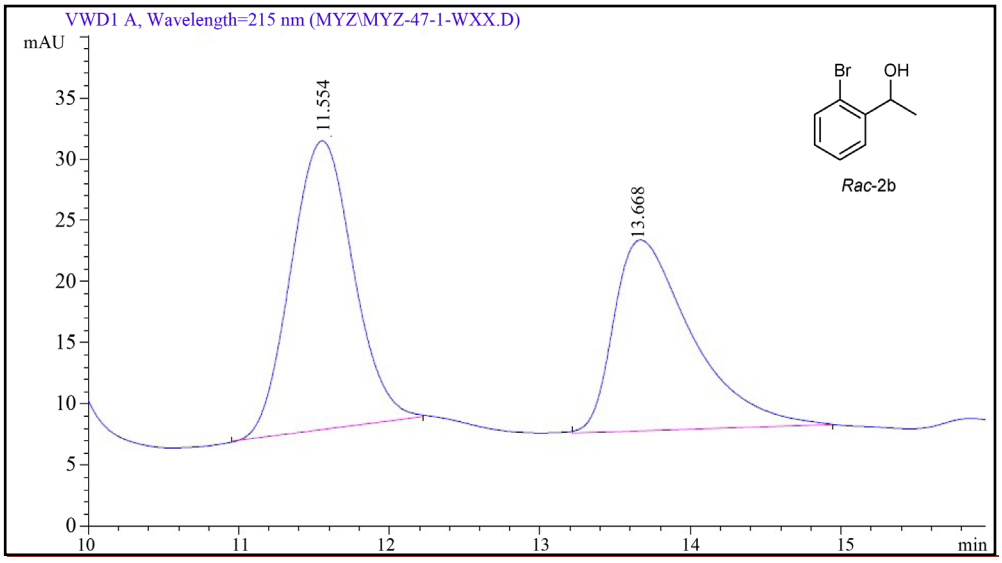

#	Time	Peak area	Peak height	Peak width	Symmetry factor	Peak area%
1	11.554	679	23.6	0.4796	0.976	54.651
2	13.668	563.4	15.6	0.6024	0.505	45.349

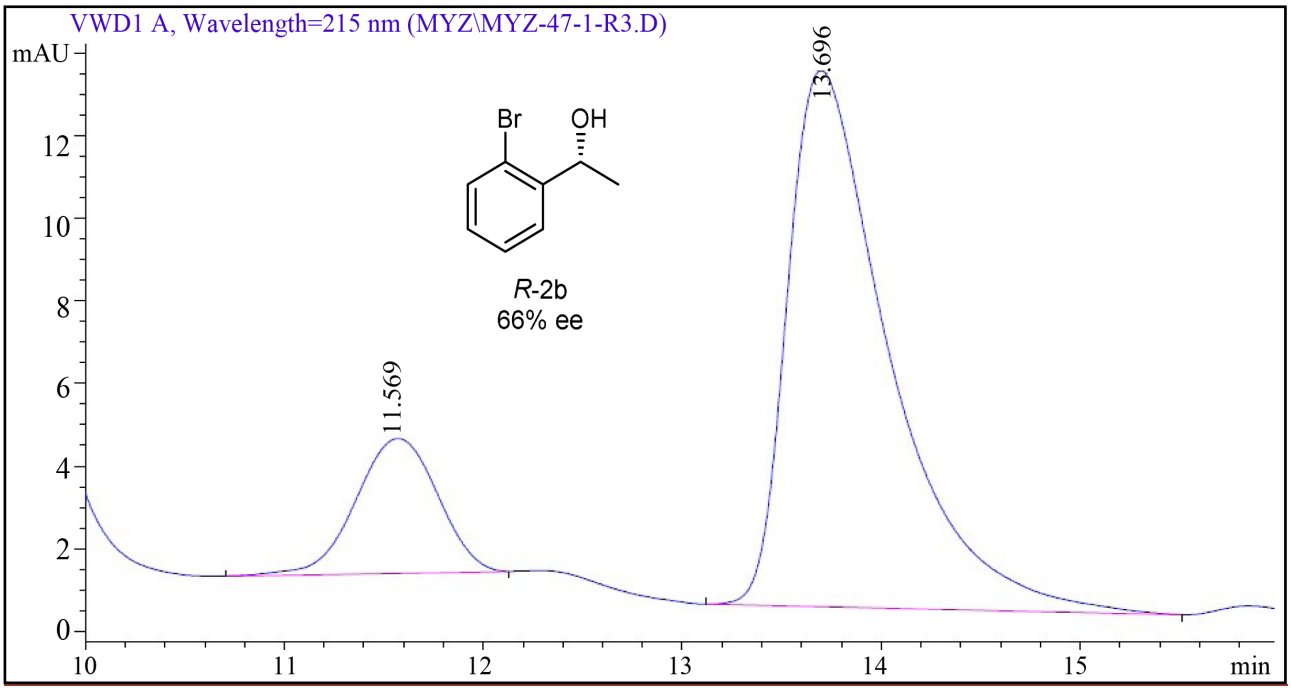

#	Time	Peak area	Peak height	Peak width	Symmetry factor	Peak area%
1	11.569	93.3	3.3	0.4526	1.054	16.828
2	13.696	461.3	13	0.5295	0.457	83.172

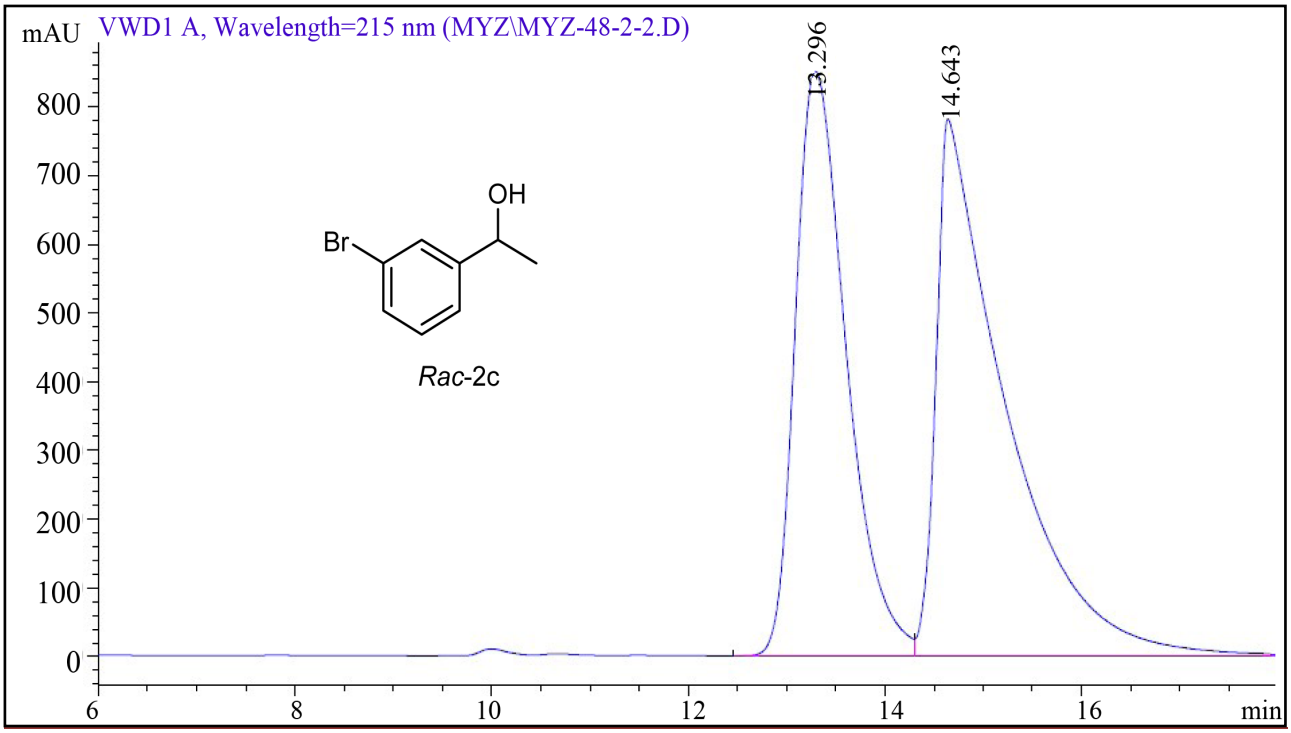

#	Time	Peak area	Peak height	Peak width	Symmetry factor	Peak area%
1	13.296	30798.1	851.2	0.5581	0.616	44.3703
2	14.643	38652.3	783.3	0.6557	0.21	55.629

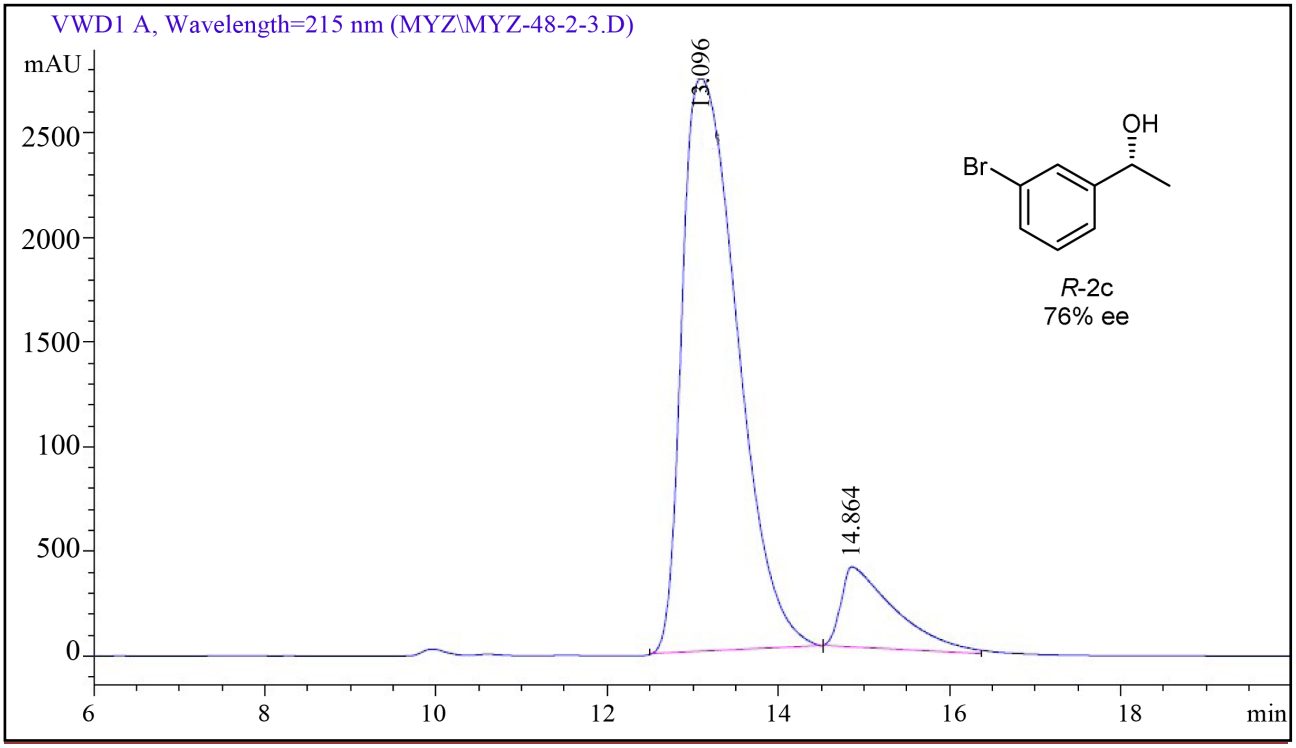

#	Time	Peak area	Peak height	Peak width	Symmetry factor	Peak area%
1	13.096	122875.1	2735.4	0.747	0.511	88.062
2	14.864	16658.2	381.5	0.7278	0.253	11.938

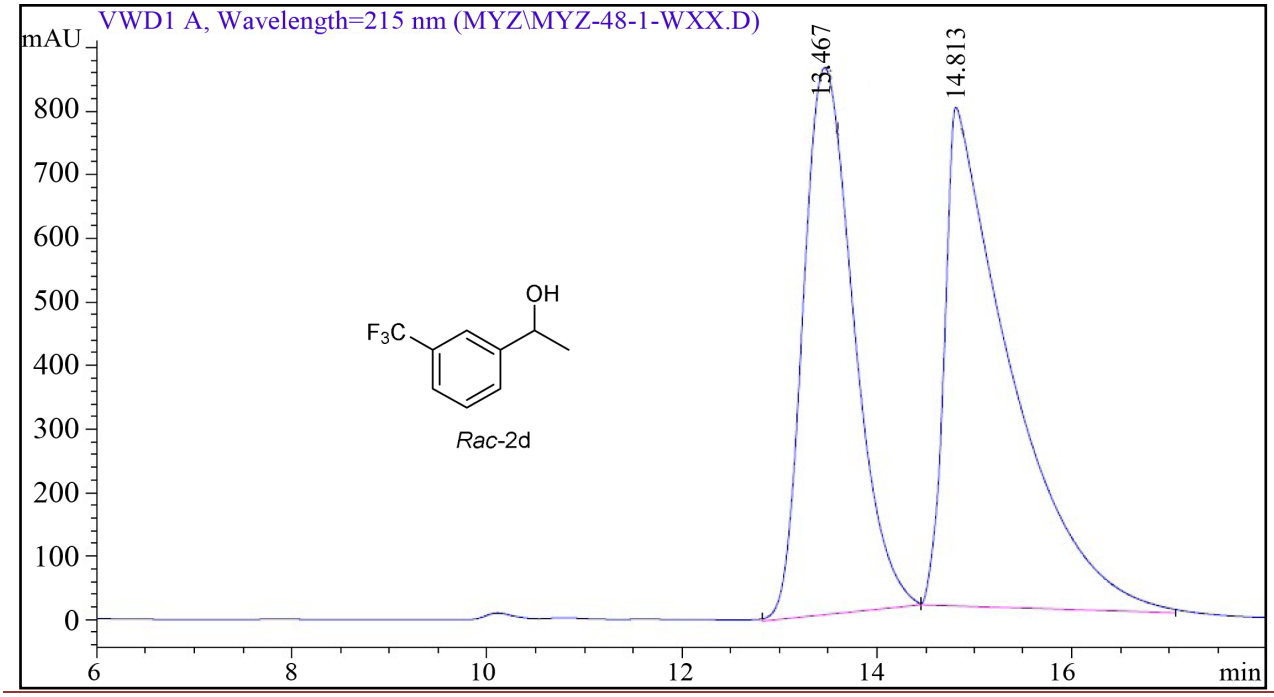

#	Time	Peak area	Peak height	Peak width	Symmetry factor	Peak area%
1	13.467	30949.6	860.3	0.5996	0.697	45.571
2	14.813	36965.2	784.4	0.7854	0.218	54.429

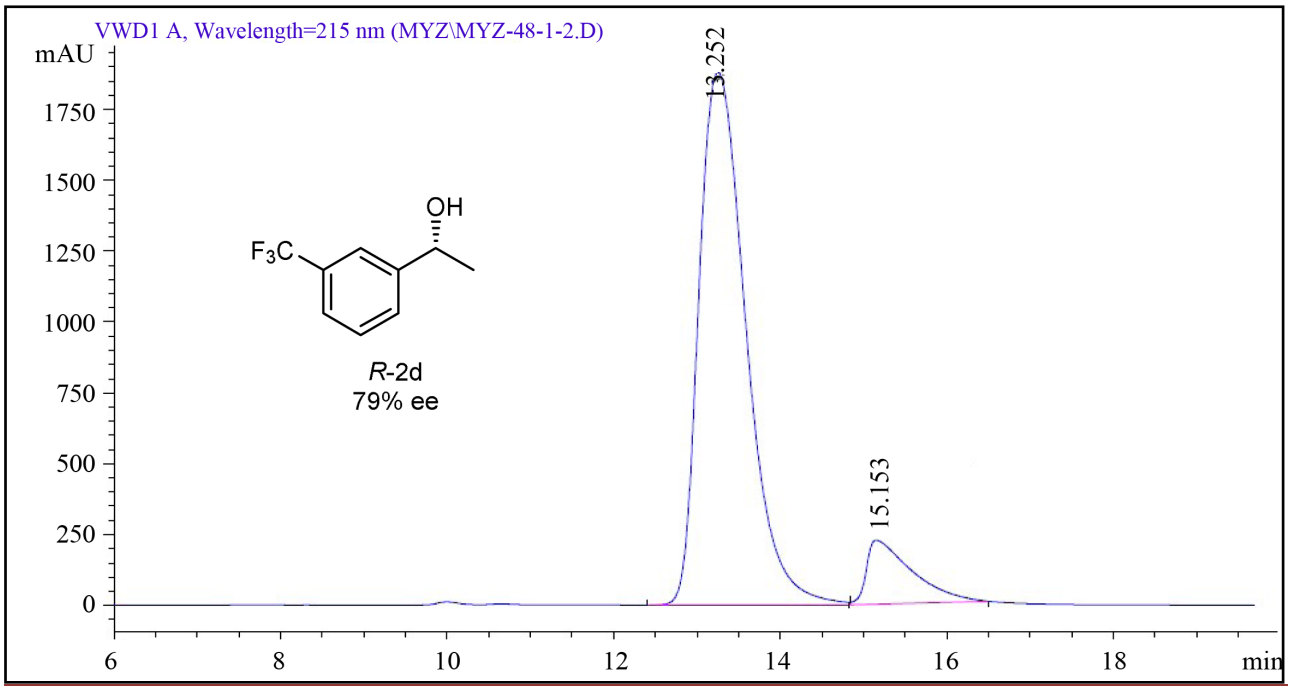

#	Time	Peak area	Peak height	Peak width	Symmetry factor	Peak area%
1	13.253	73737.2	1880.8	0.6174	0.631	89.589
2	15.153	8569.5	226	0.632	0.287	10.411

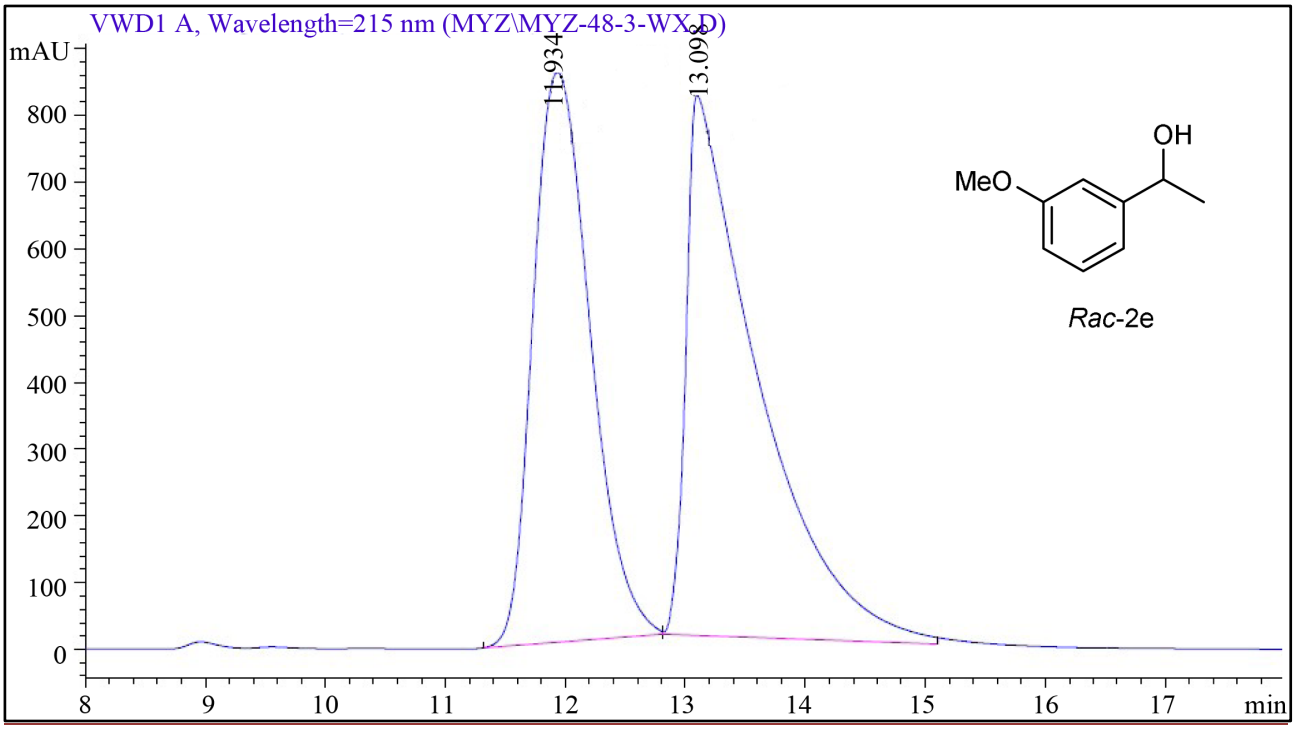

#	Time	Peak area	Peak height	Peak width	Symmetry factor	Peak area%
1	11.934	28313.5	854.6	0.5522	0.739	45.574
2	13.098	33813.1	809.8	0.6959	0.178	54.426

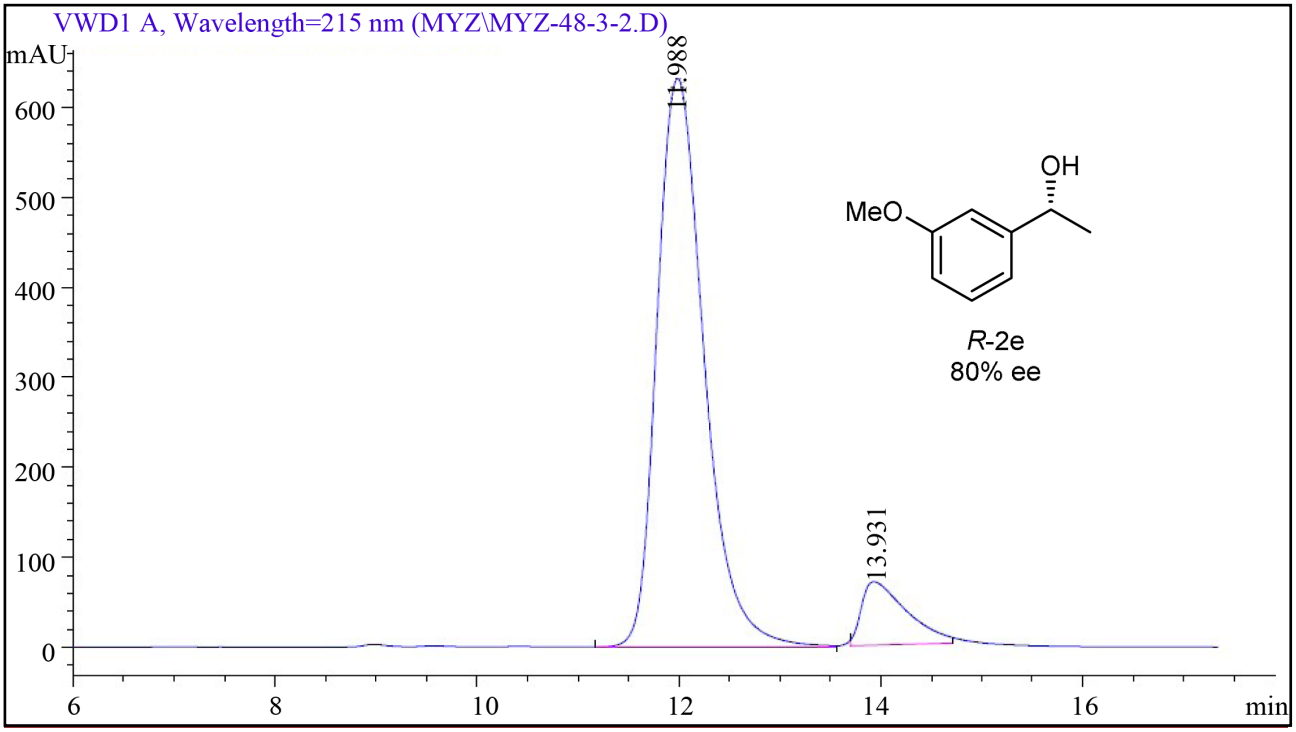

#	Time	Peak area	Peak height	Peak width	Symmetry factor	Peak area%
1	11.988	20080.9	628.9	0.532	0.717	90.119
2	13.932	2201.7	68.2	0.538	0.341	9.881

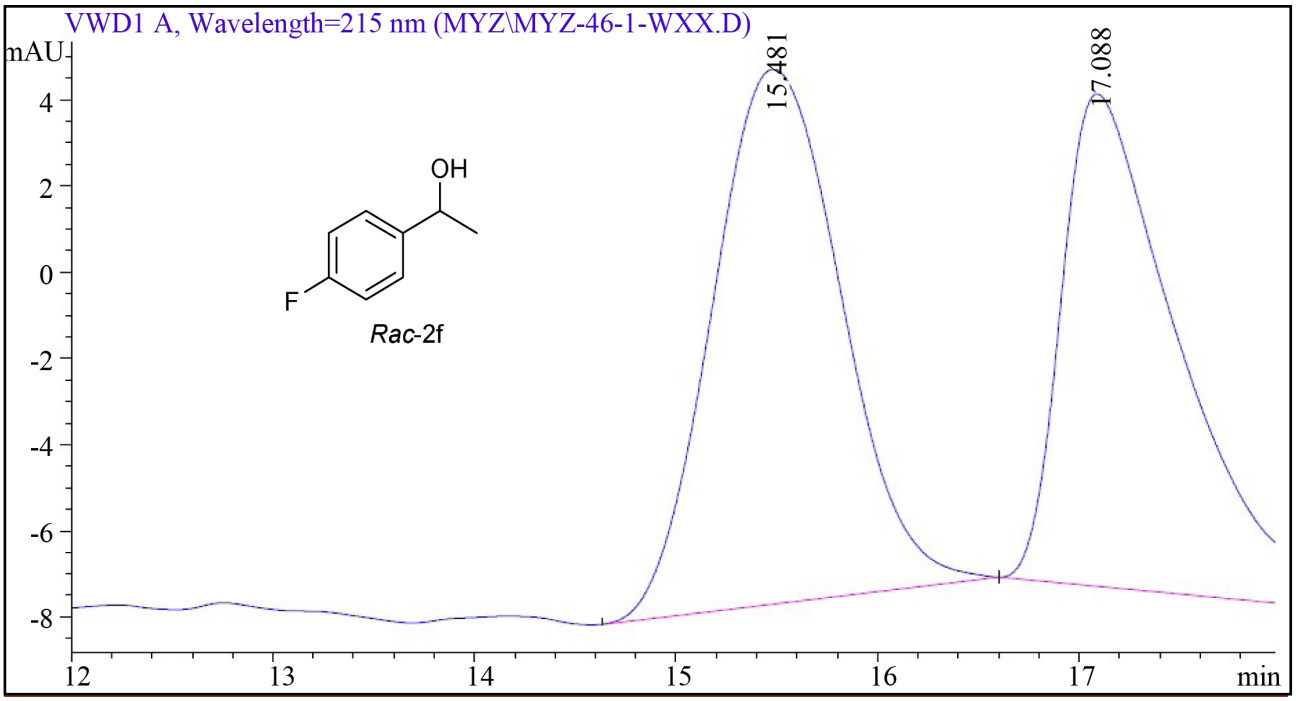

#	Time	Peak area	Peak height	Peak width	Symmetry factor	Peak area%
1	15.481	551.4	12.4	0.6982	0.868	53.340
2	17.088	482.3	11.4	0.6074	0.385	46.660

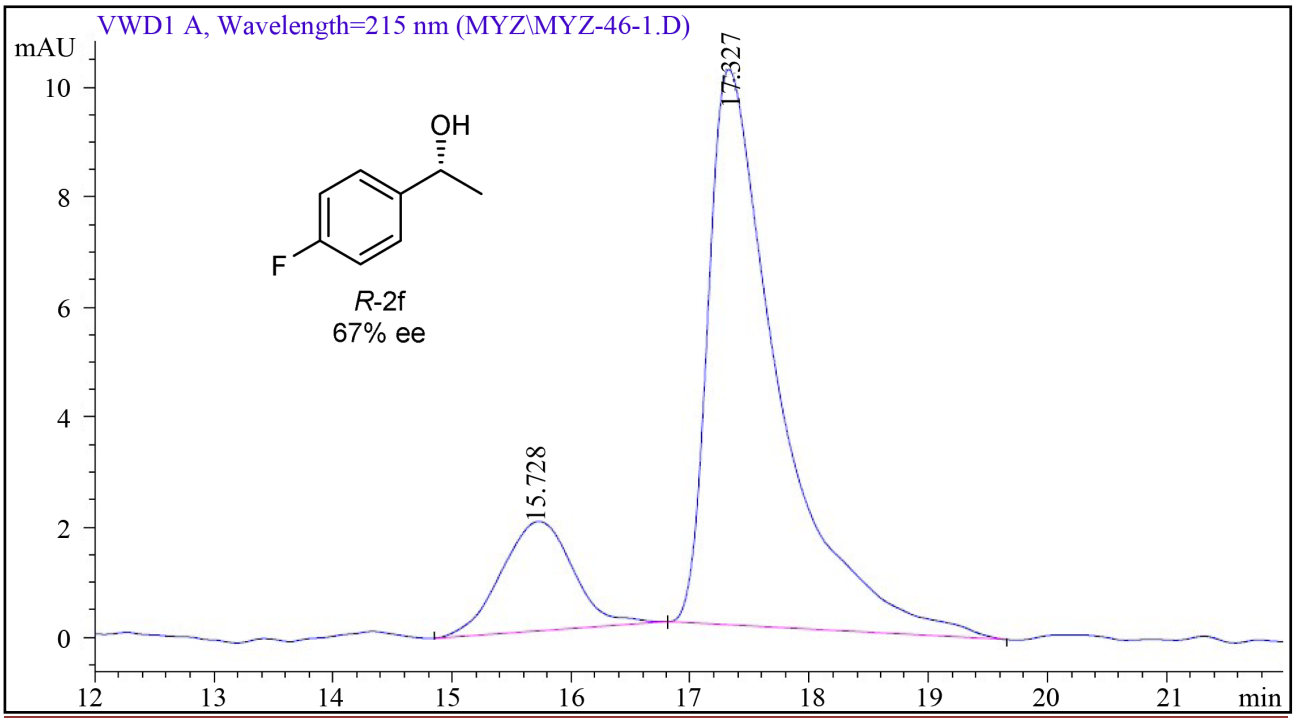

#	Time	Peak area	Peak height	Peak width	Symmetry factor	Peak area%
1	15.728	83.5	2	0.6044	1.034	16.703
2	17.327	416.4	10.1	0.5859	0.379	83.297

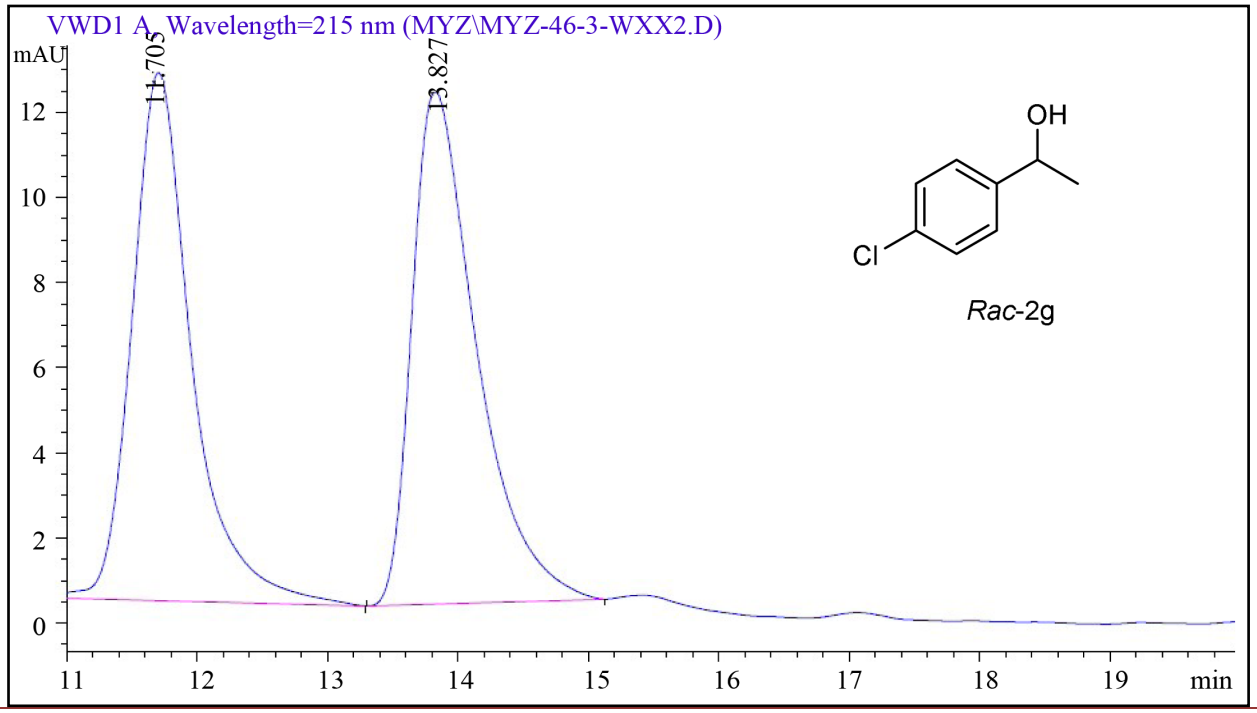

#	Time	Peak area	Peak height	Peak width	Symmetry factor	Peak area%
1	11.705	396.3	12.4	0.4755	0.737	48.865
2	13.827	414.7	12.1	0.5104	0.517	51.135

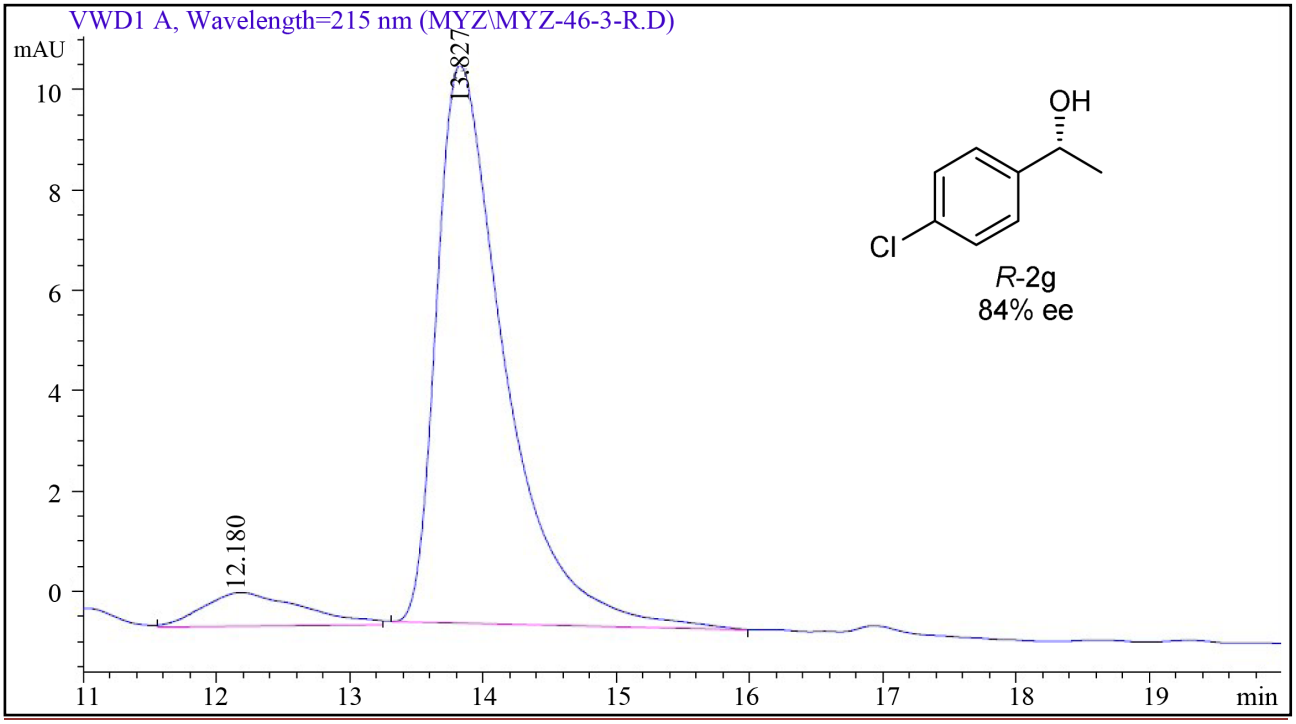

#	Time	Peak area	Peak height	Peak width	Symmetry factor	Peak area%
1	12.18	35.1	1	0.8679	0.595	8.137
2	13.827	396	11.1	0.5276	0.474	91.863

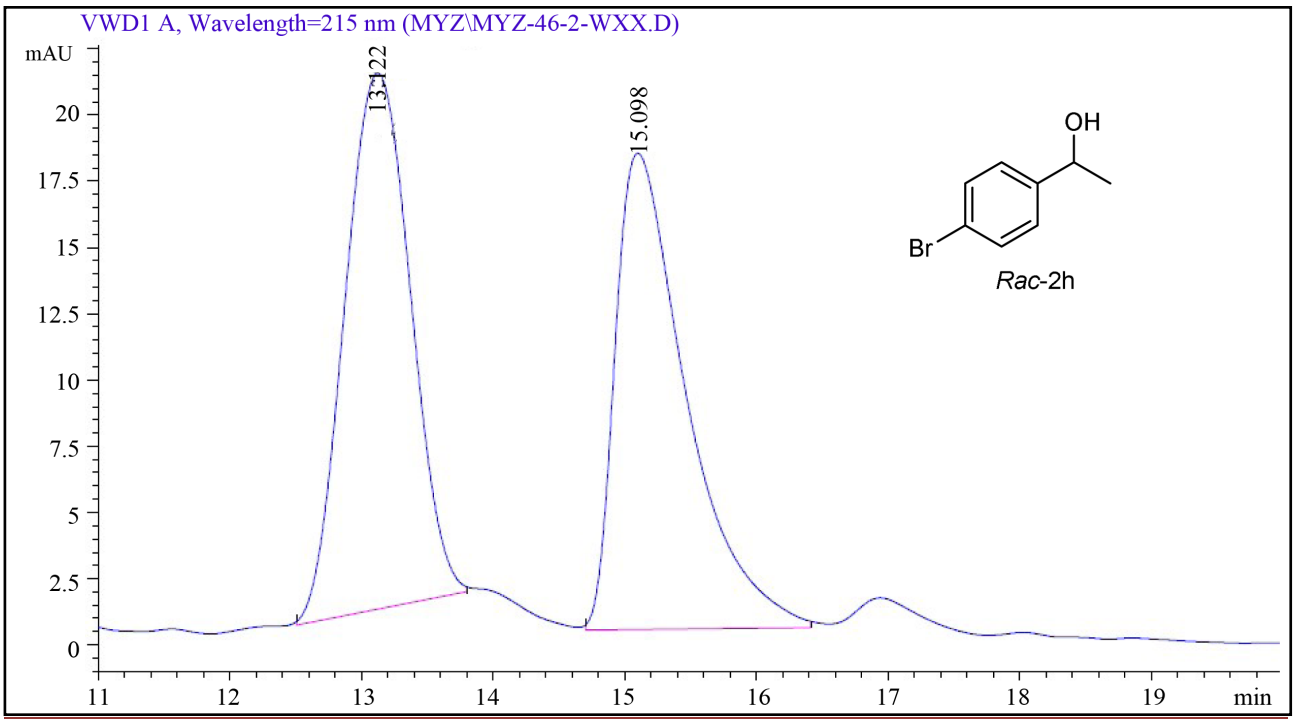

#	Time	Peak area	Peak height	Peak width	Symmetry factor	Peak area%
1	13.122	702.3	20.2	0.5787	0.977	51.024
2	15.098	674.1	18	0.625	0.451	48.976

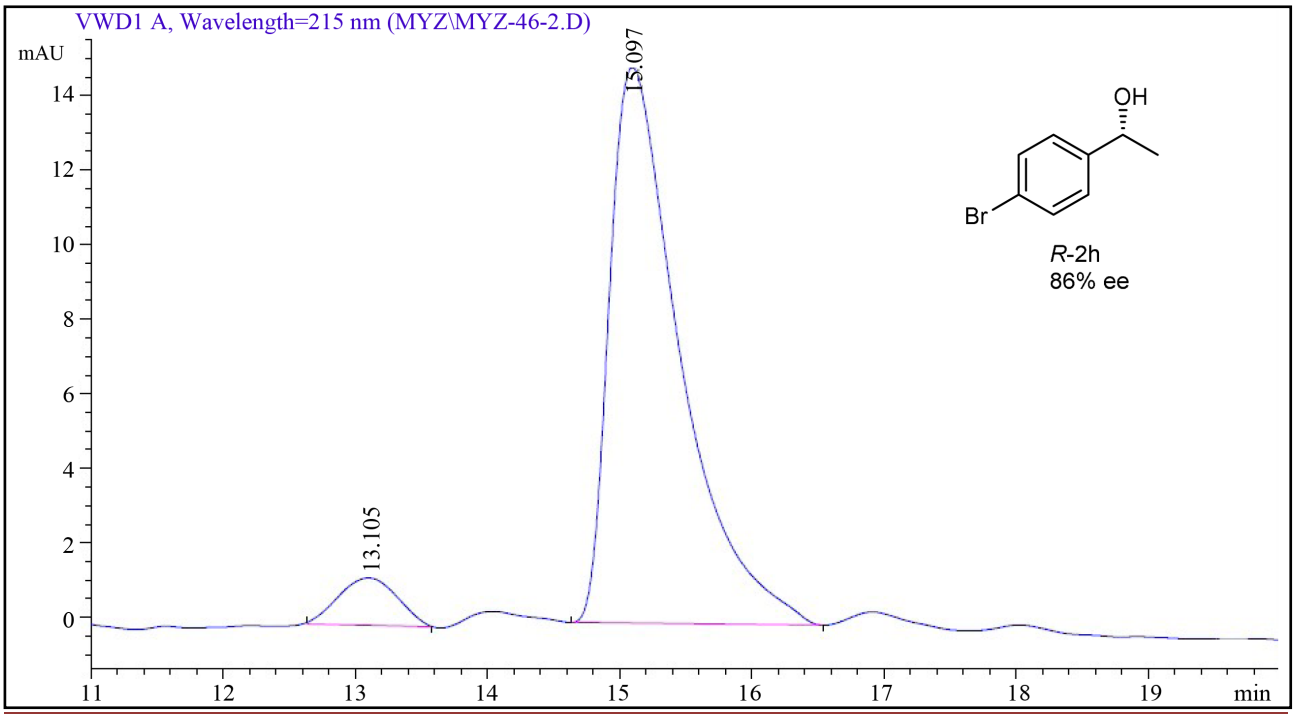

#	Time	Peak area	Peak height	Peak width	Symmetry factor	Peak area%
1	13.118	41.8	1.3	0.5369	0.768	6.991
2	15.097	556	14.9	0.5539	0.435	93.009

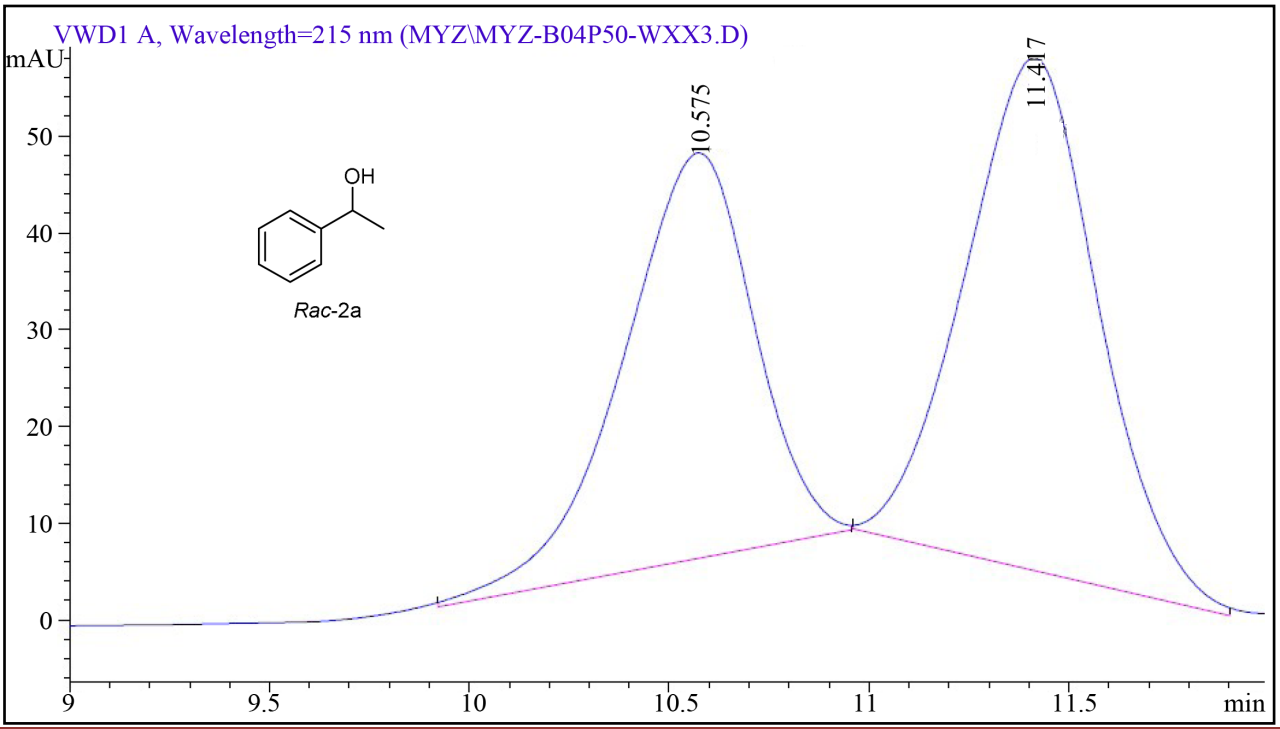

#	Time	Peak area	Peak height	Peak width	Symmetry factor	Peak area%
1	10.575	955.4	41.9	0.3803	1.352	43.628
2	11.417	1234.5	53	0.3882	1.022	56.372

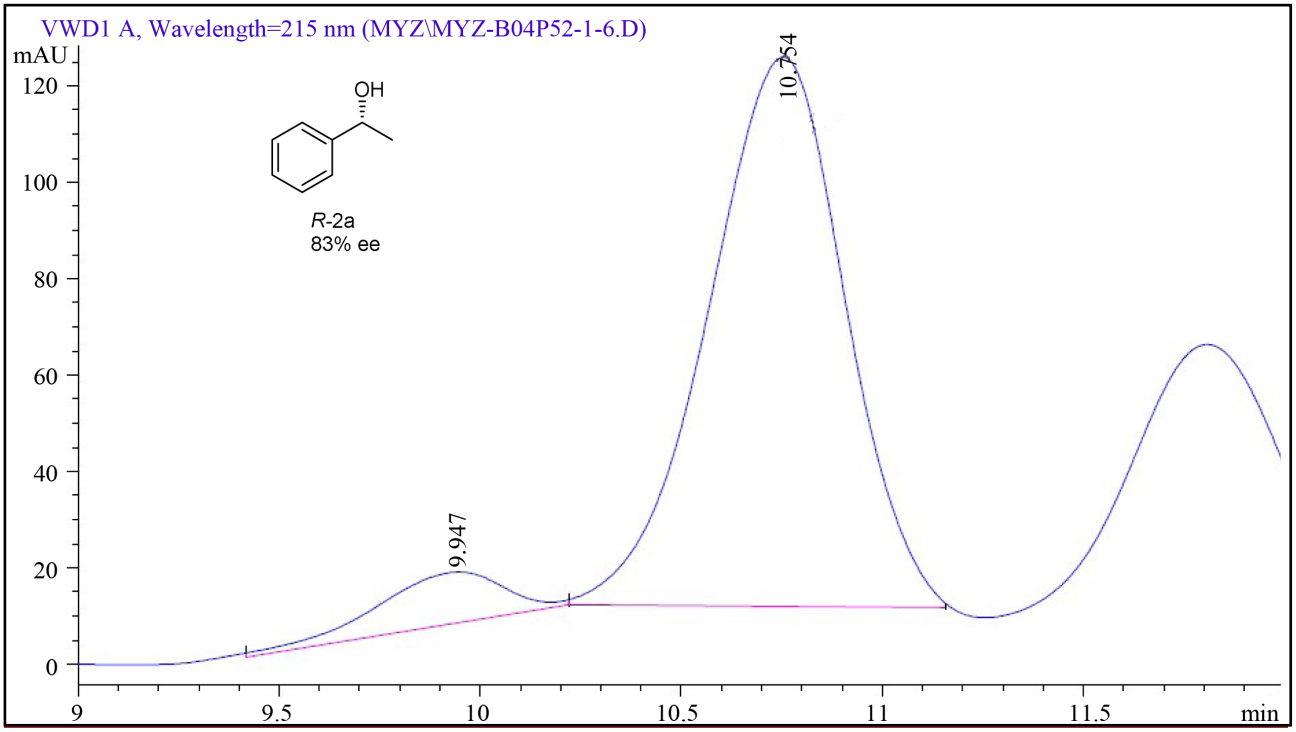

#	Time	Peak area	Peak height	Peak width	Symmetry factor	Peak area%
1	9.947	241.8	10.5	0.3825	1.953	8.267
2	10.754	2683.5	113.9	0.3926	1.176	91.733

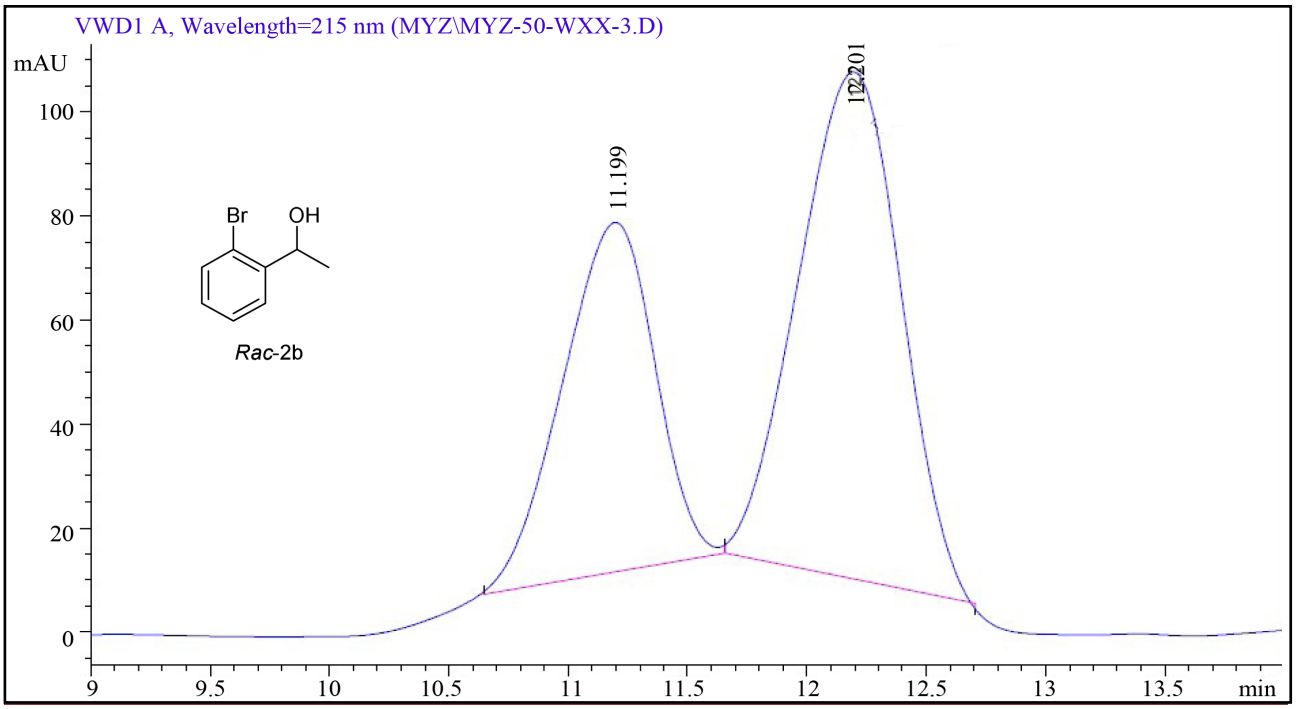

#	Time	Peak area	Peak height	Peak width	Symmetry factor	Peak area%
1	11.199	1816.2	67.2	0.4505	0.818	38.377
2	12.201	2916.4	97.5	0.4986	0.712	61.622

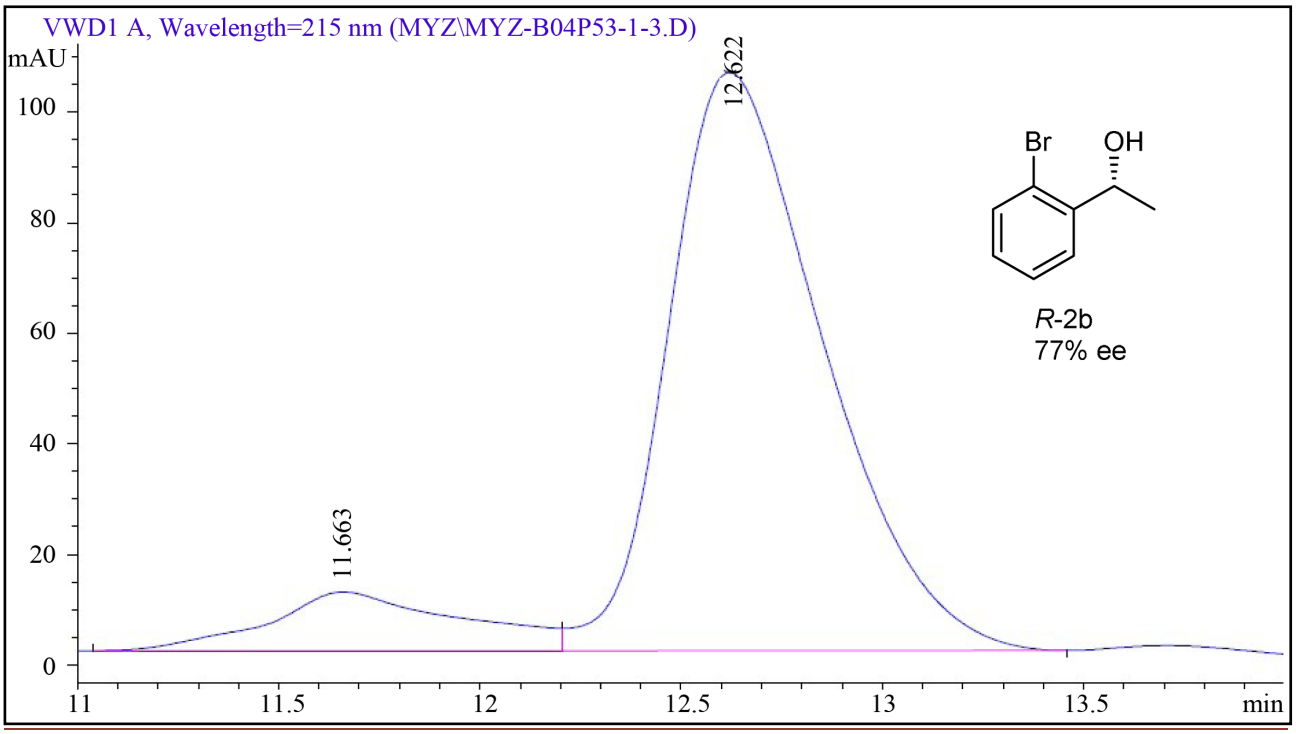

#	Time	Peak area	Peak height	Peak width	Symmetry factor	Peak area%
1	11.663	379.9	11	0.4614	0.619	11.640
2	12.622	2883.6	105.6	0.4147	0.612	88.360

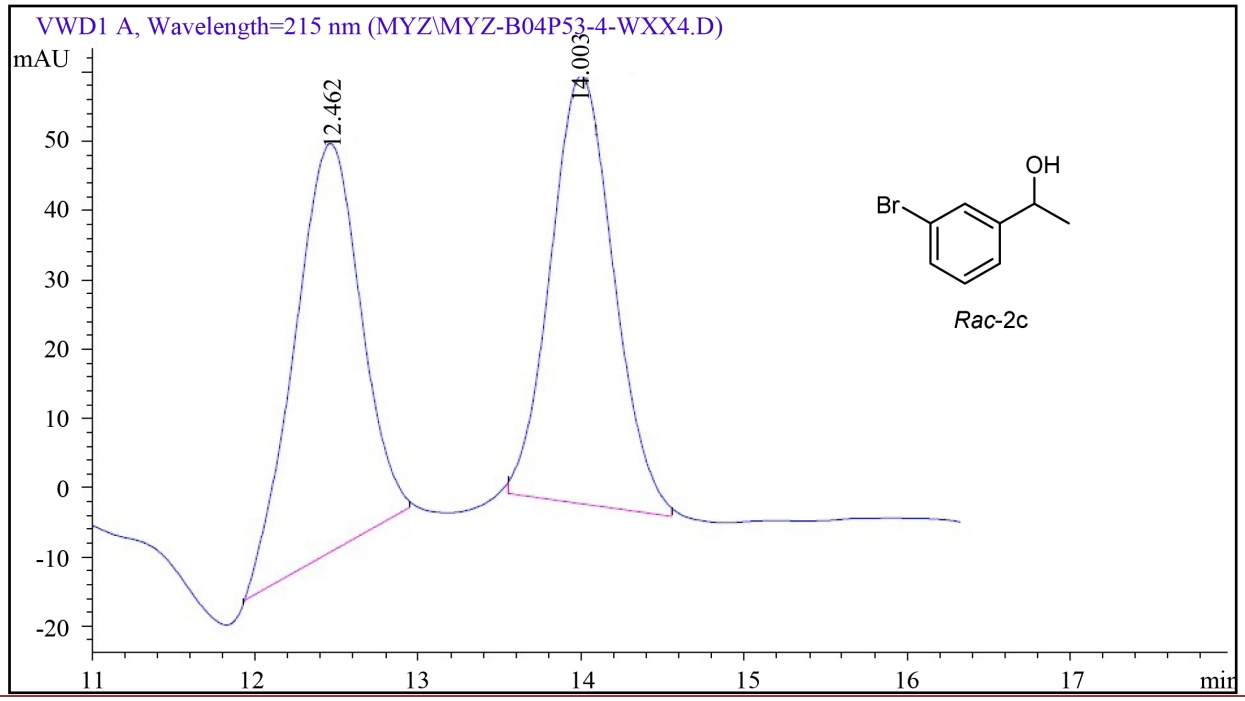

#	Time	Peak area	Peak height	Peak width	Symmetry factor	Peak area%
1	12.462	1674	59	0.4731	1.191	50.192
2	14.00.	1661.2	61.8	0.4479	0.9	49.808

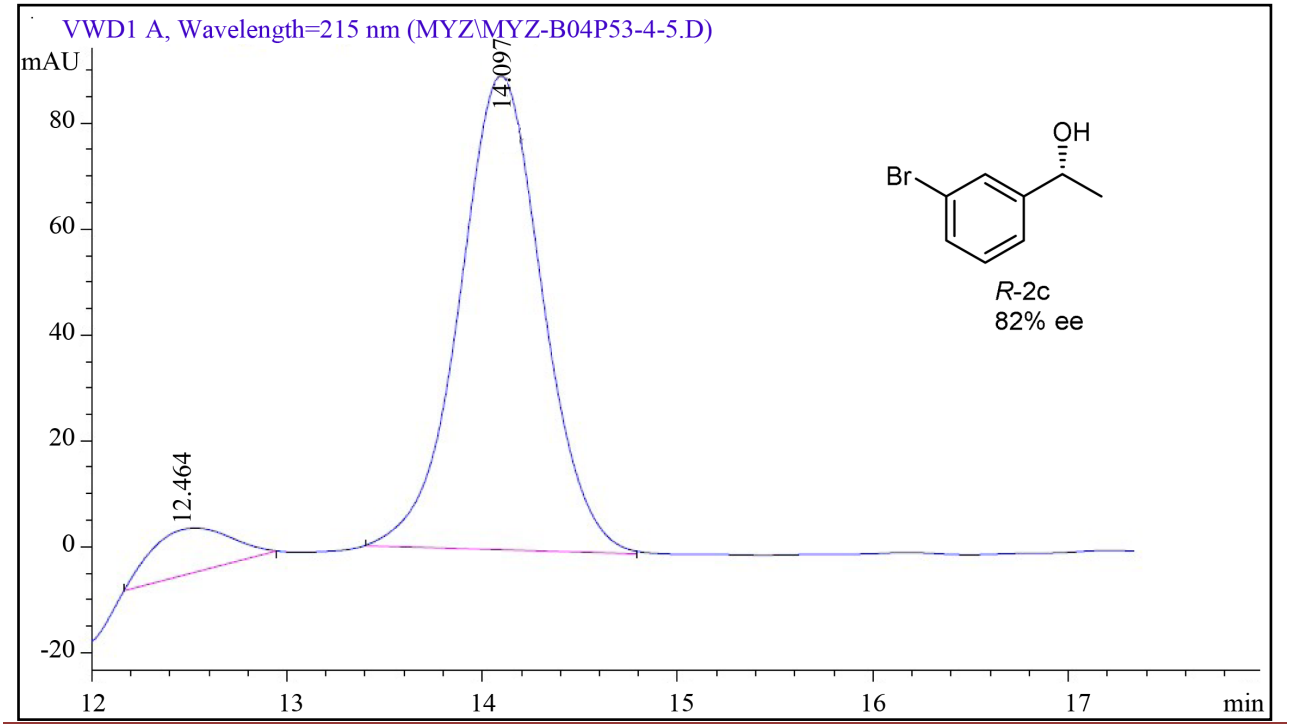

#	Time	Peak area	Peak height	Peak width	Symmetry factor	Peak area%
1	12.464	240.8	8.6	0.4644	0	8.353
2	14.097	2642.5	89.6	0.4915	0.973	91.647

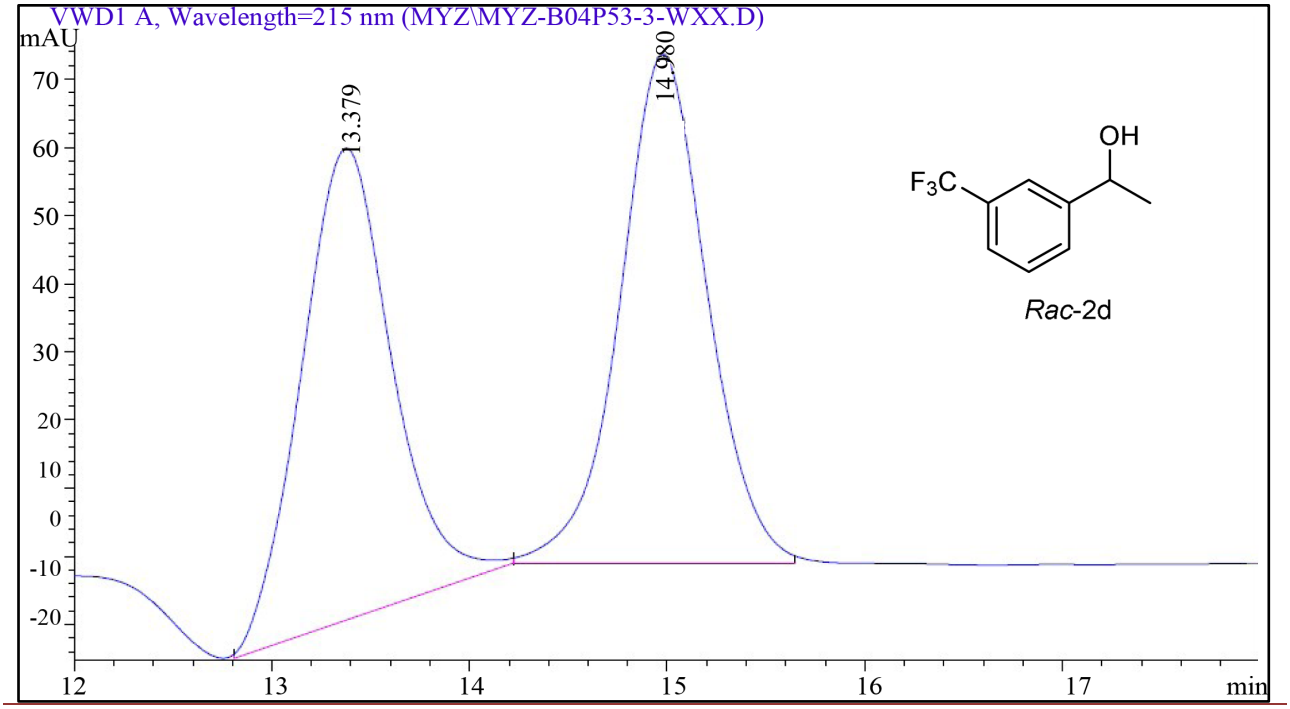

#	Time	Peak area	Peak height	Peak width	Symmetry factor	Peak area%
1	13.379	2212.1	69.3	0.5323	0.969	49.152
2	14.98	2288.3	74.6	0.5144	0.954	50.848

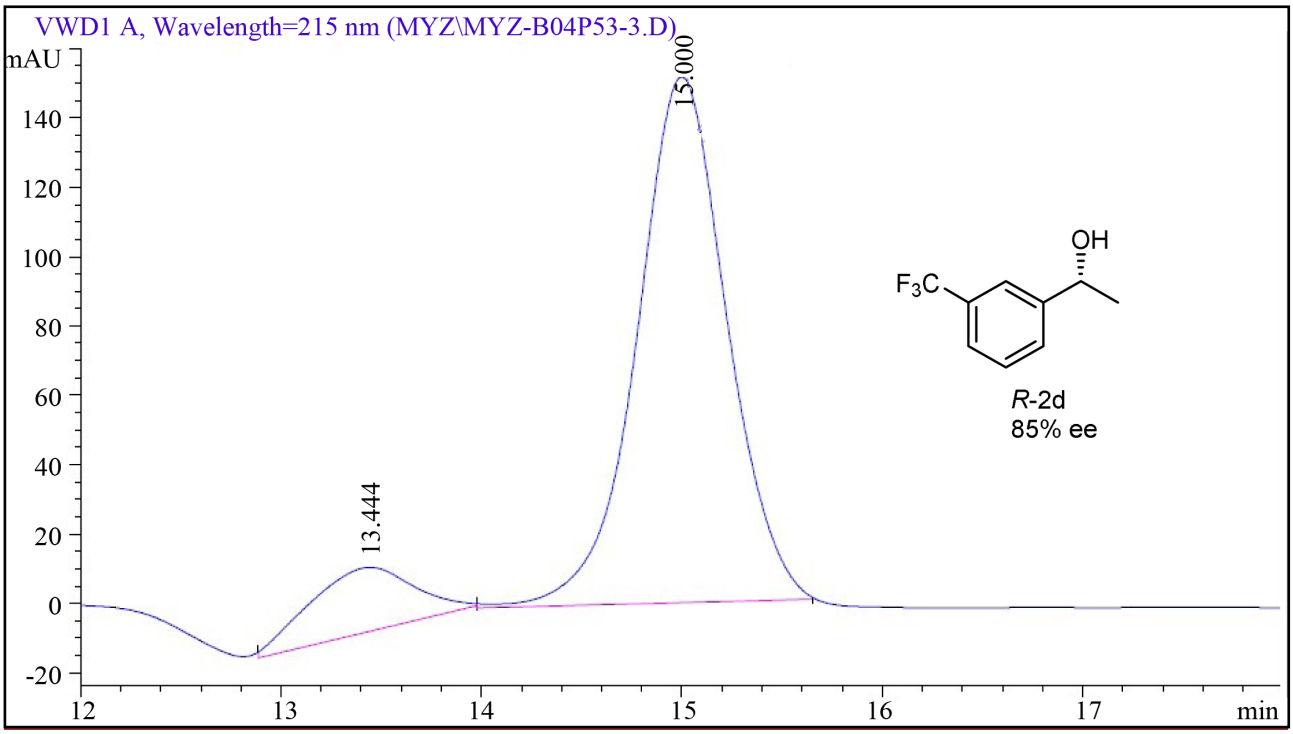

#	Time	Peak area	Peak height	Peak width	Symmetry factor	Peak area%
1	13.444	382	13.1	0.4861	0.888	7.499
2	15.000	4712.1	151.6	0.5179	0.979	92.501

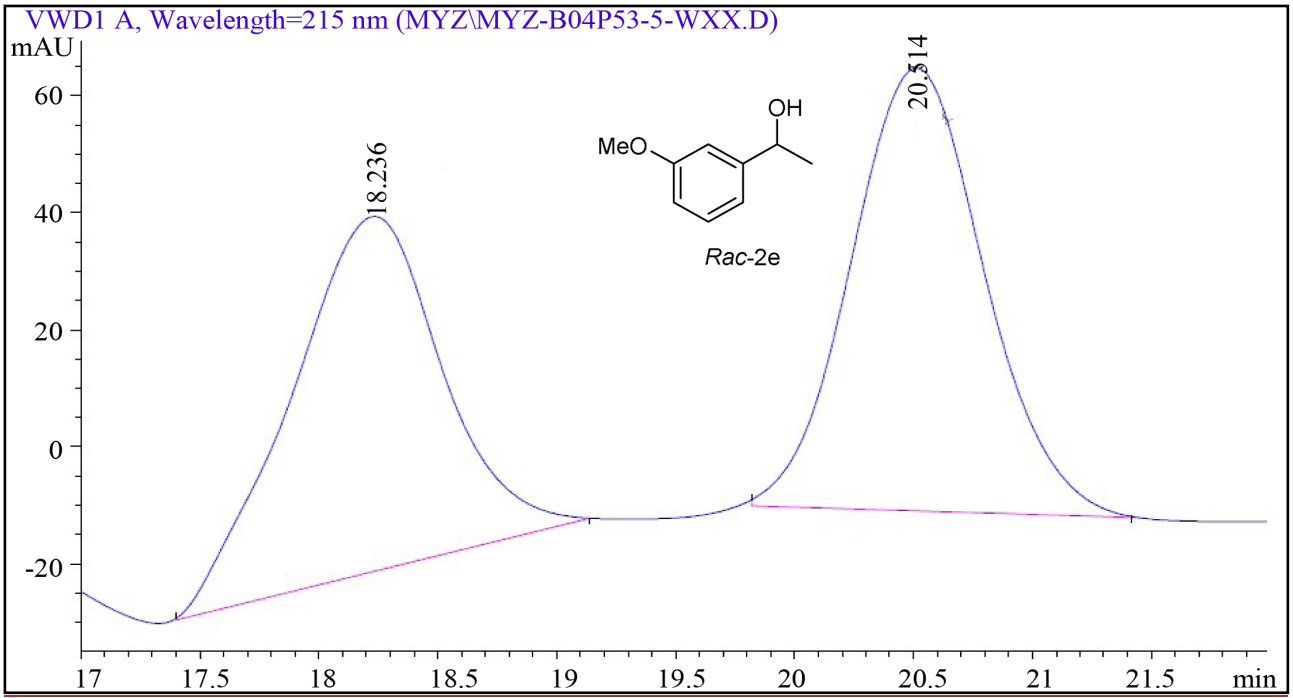

#	Time	Peak area	Peak height	Peak width	Symmetry factor	Peak area%
1	18.236	2678.6	60.6	0.7364	1.221	47.672
2	20.514	2940.3	75.7	0.6477	0.934	2.328

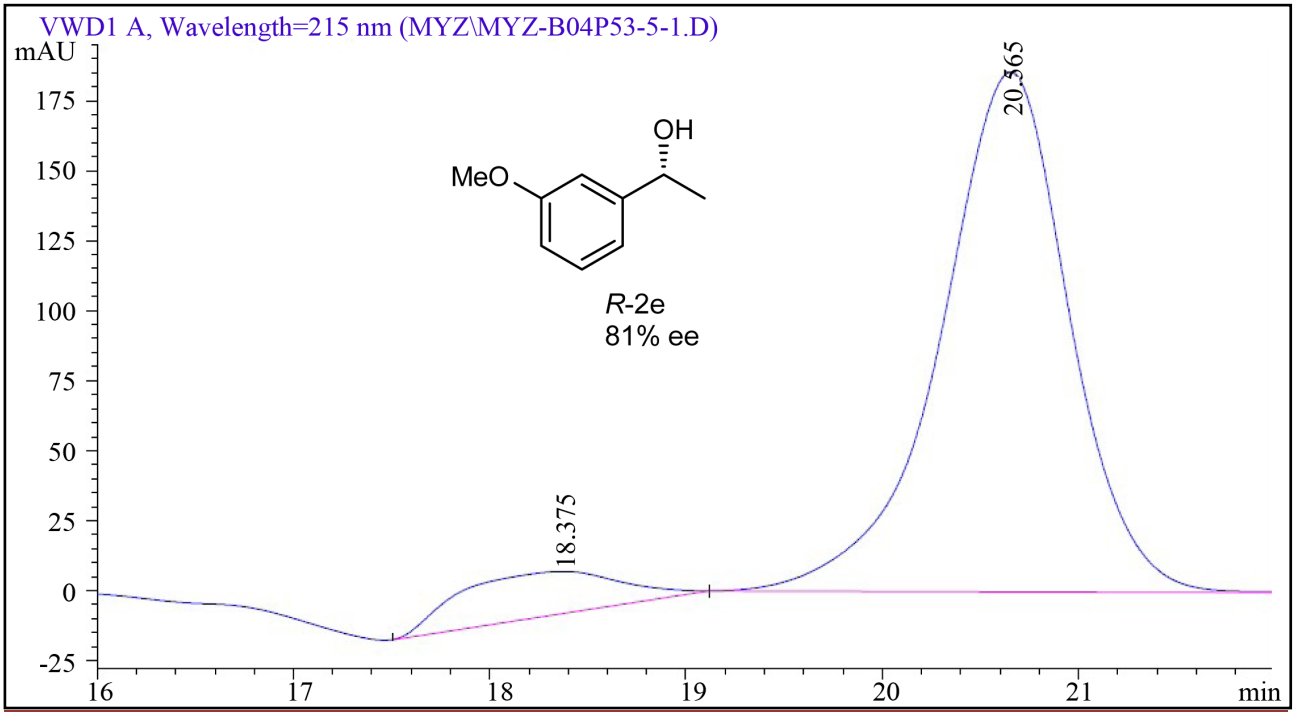

#	Time	Peak area	Peak height	Peak width	Symmetry factor	Peak area%
1	18.375	909.9	15	0.98	1.899	9.687
2	20.656	8483.4	185.6	0.6921	1.165	90.313

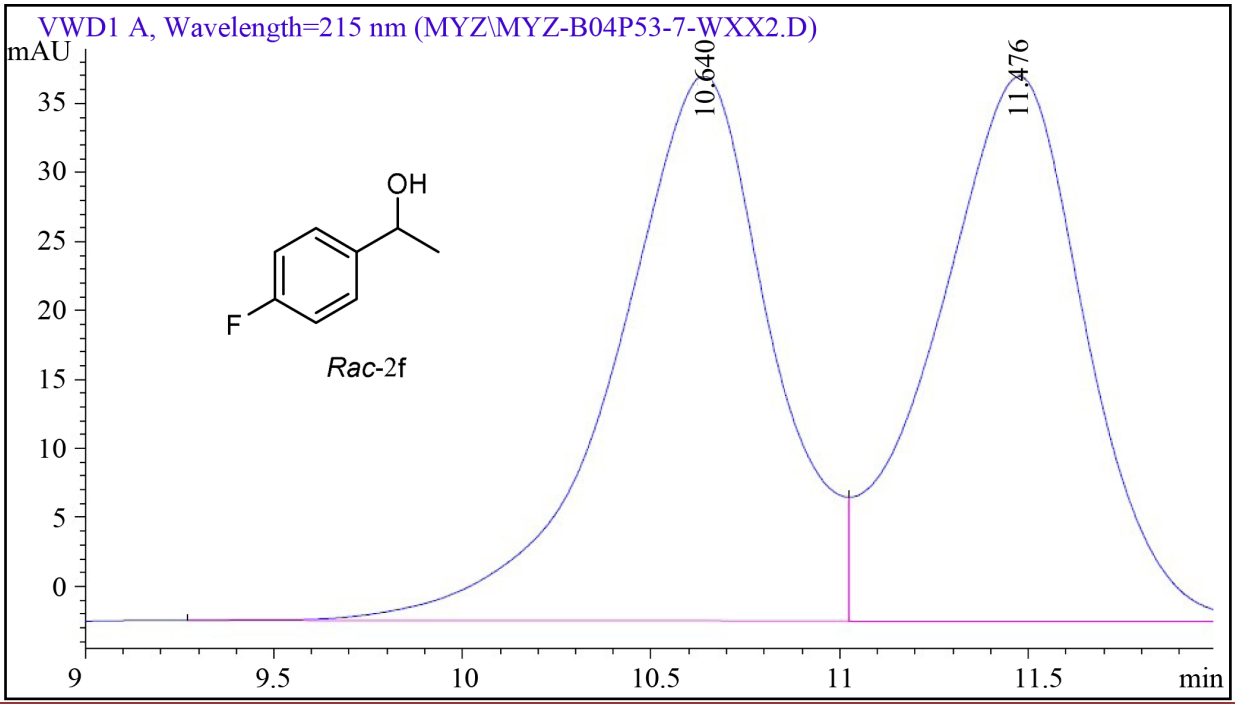

#	Time	Peak area	Peak height	Peak width	Symmetry factor	Peak area%
1	10.64	767.9	33	0.3874	1.36	48.329
2	11.484	821	34.5	0.3971	1.044	51.671

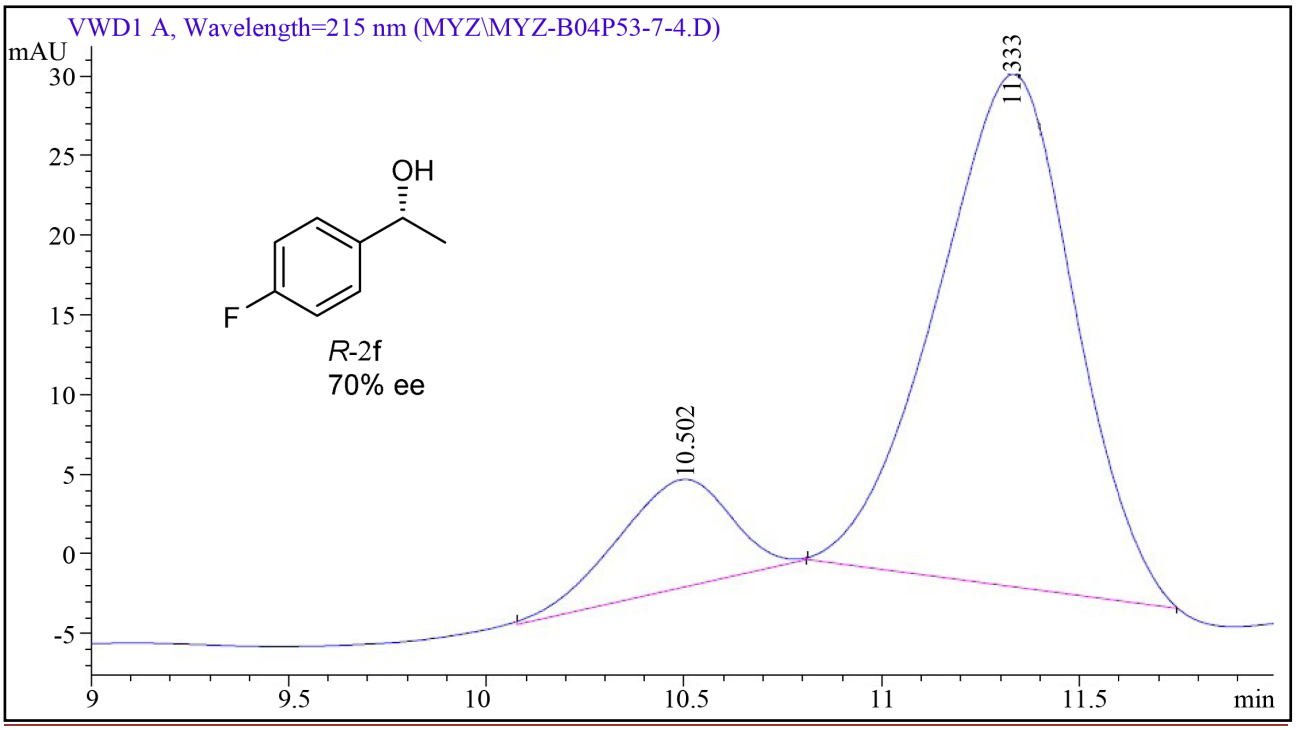

#	Time	Peak area	Peak height	Peak width	Symmetry factor	Peak area%
1	10.502	136.3	6.8	0.3363	1.541	14.868
2	11.333	780.2	32.2	0.4042	1.197	85.132

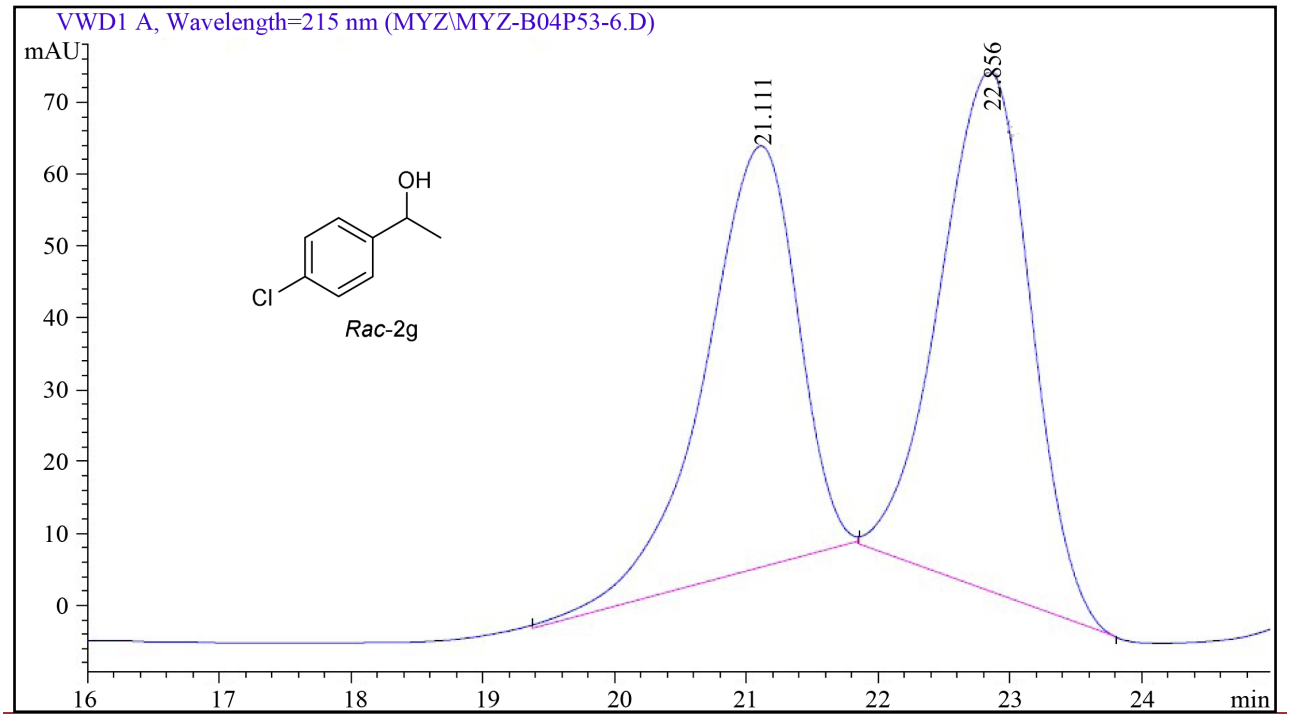

#	Time	Peak area	Peak height	Peak width	Symmetry factor	Peak area%
1	21.111	2896.9	58.6	0.8234	1.52	45.474
2	22.856	3473.5	72.3	0.801	1.155	54.526

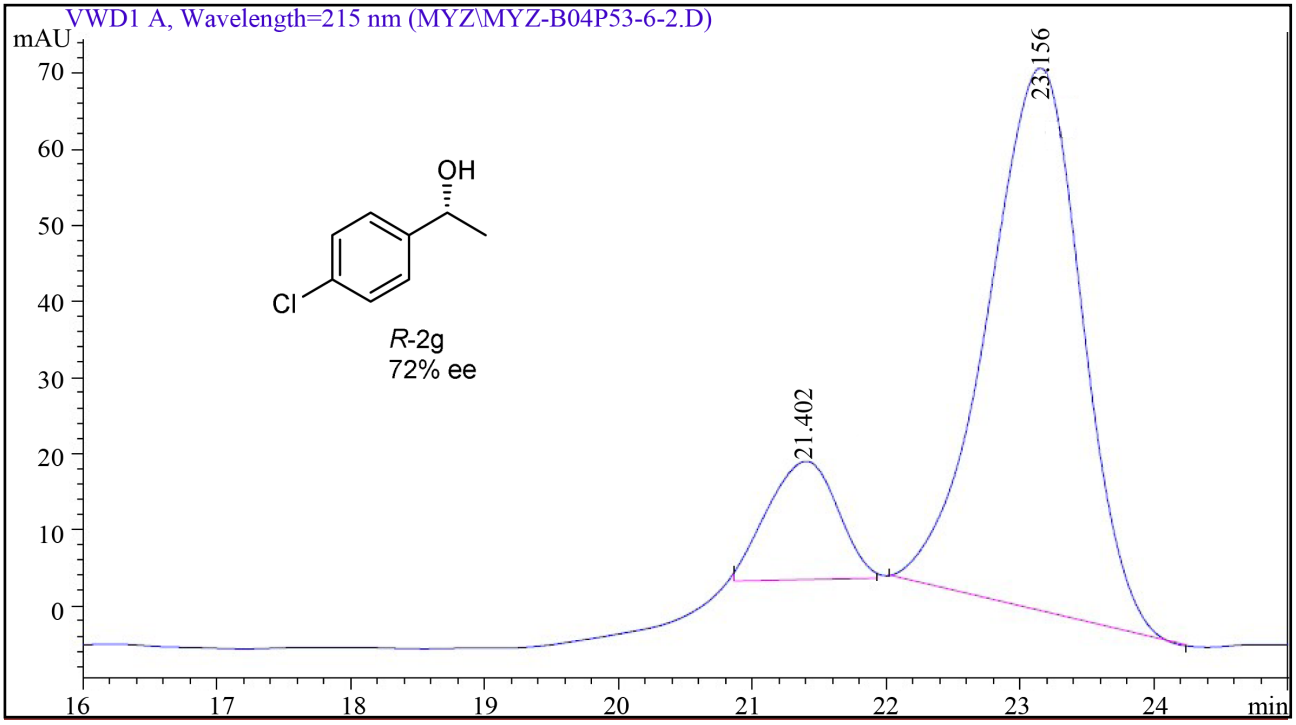

#	Time	Peak area	Peak height	Peak width	Symmetry factor	Peak area%
1	21.402	573.7	15.6	0.6118	1.198	14.014
2	23.156	3520.1	71.6	0.8191	1.207	85.986

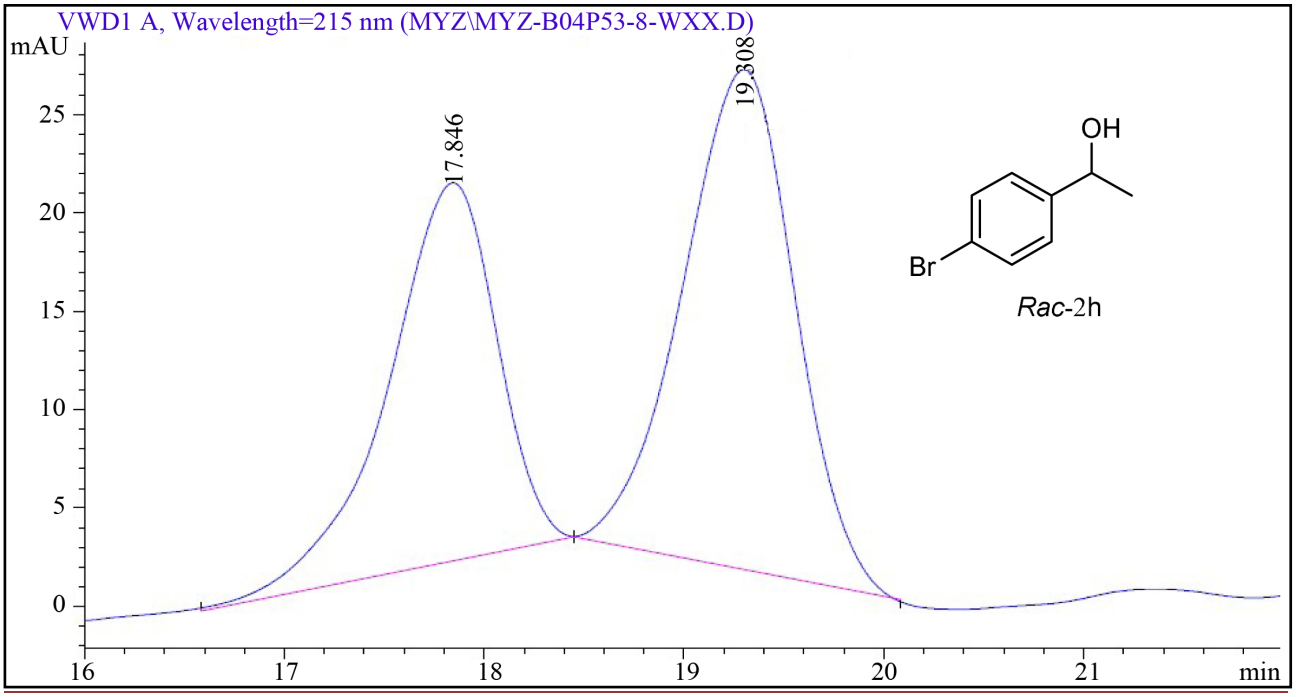

#	Time	Peak area	Peak height	Peak width	Symmetry factor	Peak area%
1	17.846	729	19.2	0.6329	1.474	42.326
2	19.308	993.3	25.4	0.6519	1.152	57.674

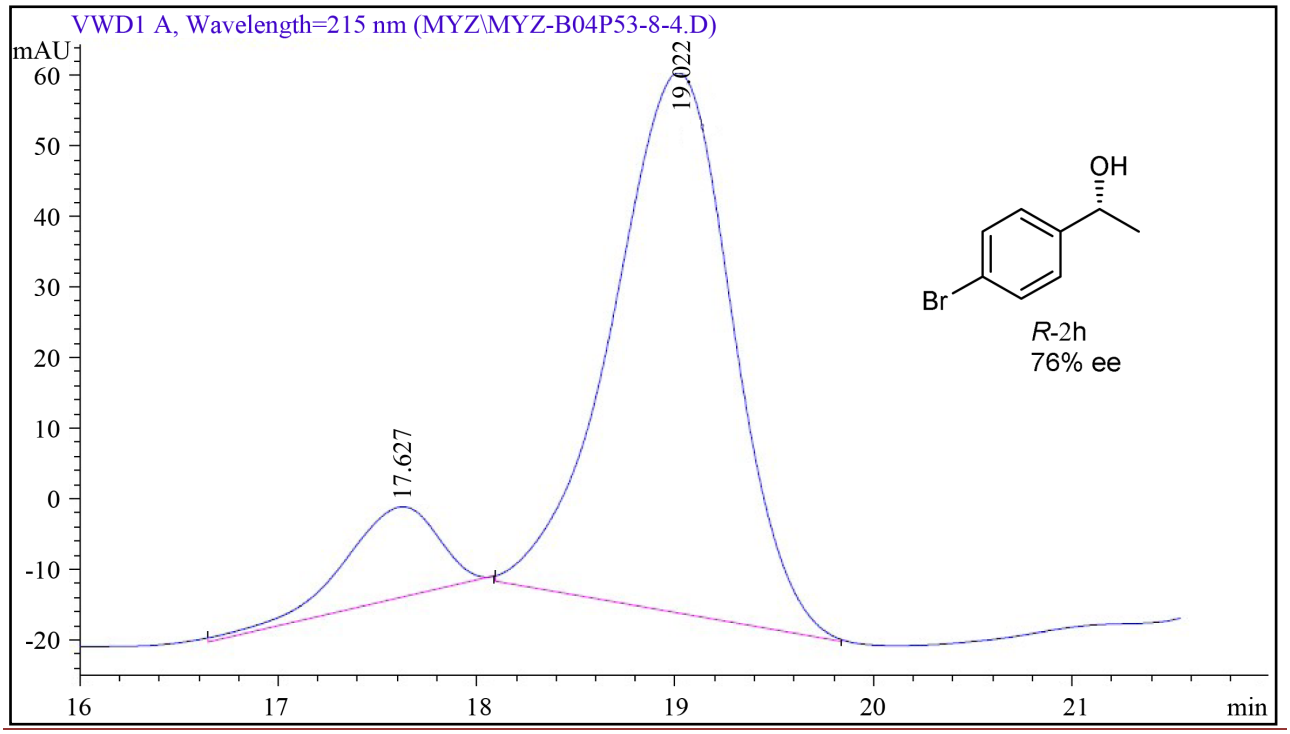

#	Time	Peak area	Peak height	Peak width	Symmetry factor	Peak area%
1	17.627	427.2	12.8	0.5551	1.741	11.747
2	19.016	3209.4	76.6	0.6981	1.334	88.253